

# Form factors of $B \rightarrow \pi \ell \nu$ and a determination of $|V_{ub}|$ with Möbius domain-wall fermions

Brian Colquhoun<sup>1,2,\*</sup>, Shoji Hashimoto<sup>2,3,†</sup>, Takashi Kaneko<sup>2,3,5,‡</sup> and Jonna Koponen<sup>4,2,§</sup>

(JLQCD Collaboration)

<sup>1</sup>*Department of Physics and Astronomy, York University, Toronto, Ontario M1J 1P3, Canada*

<sup>2</sup>*High Energy Accelerator Research Organization (KEK), Tsukuba 305-0801, Japan*

<sup>3</sup>*School of High Energy Accelerator Science, SOKENDAI (The Graduate University for Advanced Studies), Tsukuba 305-0801, Japan*

<sup>4</sup>*PRISMA+ Cluster of Excellence & Institut für Kernphysik, Johannes Gutenberg-Universität Mainz, D-55128 Mainz, Germany*

<sup>5</sup>*Kobayashi-Maskawa Institute for the Origin of Particles and the Universe, Nagoya University, Nagoya, Aichi 464-8602, Japan*



(Received 18 March 2022; accepted 11 August 2022; published 6 September 2022)

Using a fully relativistic lattice fermion action, we compute the form factors of the semileptonic decay  $B \rightarrow \pi \ell \nu$ , which is required for the determination of the Cabibbo-Kobayashi-Maskawa matrix element  $|V_{ub}|$ . We employ the Möbius domain-wall fermion formalism for the generation of lattice ensembles with  $2 + 1$  sea quark flavors as well as for the valence heavy and light quarks. We compute the form factors at various values of the lattice spacing and multiple light and heavy quark masses, and extrapolate the results to the physical point. We combine our lattice results with the available experimental data to obtain  $|V_{ub}| = (3.93 \pm 0.41) \times 10^{-3}$ .

DOI: [10.1103/PhysRevD.106.054502](https://doi.org/10.1103/PhysRevD.106.054502)

## I. INTRODUCTION

The determination of the Cabibbo-Kobayashi-Maskawa (CKM) matrix element  $|V_{ub}|$  from the measurement of the exclusive semileptonic decay  $B \rightarrow \pi \ell \nu$  requires precise knowledge of the corresponding decay form factors, which can be obtained using lattice simulations of quantum chromodynamics (QCD). For the first time in lattice QCD we calculate these quantities using a fully relativistic approach.  $|V_{ub}|$  is an important Standard Model parameter, and the ratio  $|V_{ub}|/|V_{cb}|$  is a particularly sought-after result that requires continued refining of both these elements of the CKM matrix.

Heavy quarks require special consideration in lattice QCD since, on coarse lattices, discretization errors from large masses in lattice units,  $am_Q$ , become uncontrollable. Therefore,  $B \rightarrow \pi \ell \nu$  calculations typically use effective actions for  $b$  quarks, such as nonrelativistic QCD (NRQCD) [1–3], the Columbia interpretation of relativistic heavy quarks (RHQ) [4] and the Fermilab interpretation of the Sheikholeslami-Wohlert clover action [5]. Alternatively, it is possible to use multiple values of the heavy quark mass  $am_Q < am_b$  in a fully relativistic action and extrapolate to the physical mass. This requires that sufficiently fine lattices are available to keep  $am_Q$  small enough that discretization effects can be controlled when combining the data at various lattice spacings. We take the latter approach in this work using the Möbius domain-wall fermion action [6–10]. We use the same action for the heavy and light quarks, and for both valence and sea light quarks.

With the Möbius domain-wall fermion formalism, the leading discretization effects are of  $\mathcal{O}(a^2)$ . In our analysis we extrapolate the results at finite lattice spacing to the continuum limit assuming that there are effects of  $\mathcal{O}(a^2)$  as well as a term proportional to  $(am_Q)^2$ , which is specific to the heavy quark. The maximum value of  $am_Q$  used in this work is 0.688 so that discretization effects are kept under control. The continuum extrapolation is combined with the

\*brian.colquhoun@glasgow.ac.uk

†shoji.hashimoto@kek.jp

‡takashi.kaneko@kek.jp

§jkoponen@uni-mainz.de

||Current address: SUPA, School of Physics and Astronomy, University of Glasgow, Glasgow G12 8QQ, United Kingdom.

Published by the American Physical Society under the terms of the [Creative Commons Attribution 4.0 International license](https://creativecommons.org/licenses/by/4.0/). Further distribution of this work must maintain attribution to the author(s) and the published article's title, journal citation, and DOI. Funded by SCOAP<sup>3</sup>.

extrapolation to the physical heavy and light quark masses in a global fit function. The associated systematic errors are estimated by introducing higher order dependences on the lattice spacing and quark masses.

The momentum transfer range in  $B \rightarrow \pi \ell \nu$  decays is large, owing to the large energy release from the  $b$  quark. The most precise experimentally available data points are in the small momentum transfer  $q^2 \ll m_b^2$  corresponding to the kinematics where the pion recoil momentum is large. The small recoil data near maximum momentum transfer  $q^2 \approx 26.46 \text{ GeV}^2$  is less copious and the relative statistical error is larger. On the lattice QCD side, the most accurate form factor results are obtained at large momentum transfer when the recoil momentum is small. In order to make most use of the available information from both experiment and lattice calculations, one can combine the data to constrain the  $q^2$  dependence using the so-called  $z$ -parameter expansion [11–18], as first applied to the  $B \rightarrow \pi \ell \nu$  process in Ref. [19]. This approach only makes assumptions about the analytic structure of the form factors and, because it only involves an expansion about a small parameter  $z$ , the results are robust. We follow this strategy in this work and estimate the associated errors.

In calculations of both  $|V_{cb}|$  and  $|V_{ub}|$  there exist persistent tensions between their exclusive and inclusive determinations [20,21]. The cause(s) of this tension is still unclear, although new theoretical and experimental analyses for  $|V_{cb}|$  are revealing potential problems in previous analyses, such as the assumed functional form of the form factors. A recent review of the  $|V_{cb}|$  puzzle can be found in Ref. [22], while general overviews of the CKM matrix elements from a lattice perspective can be found in Refs. [23,24].

A more elaborate analysis of  $|V_{ub}|$  is premature due to the small branching fraction, but care is needed to ensure that the choice of the parametrization of the form factors allows systematic improvement when more data becomes available. On the exclusive side, the model-independent lattice calculation is a key element in the combined analysis with experimental data. In this work we provide a fully nonperturbative computation of the  $B \rightarrow \pi \ell \nu$  form factors with controlled extrapolation to the physical mass parameters for both heavy and light quarks as well as to vanishing lattice spacing. A discussion of the inclusive determination of  $|V_{ub}|$  is beyond the scope of this paper as it involves very different theoretical methods, such as perturbative QCD and the heavy quark expansion, but we note that a promising new direction for tackling the problem using lattice QCD is also being developed [25,26].

The rest of this paper is organized as follows. In Sec. II we discuss the relevant background, including details on the form factors obtained from the calculation and how they are extracted using the appropriate matrix elements. The lattice setup and procedure for our calculation is described in Sec. III, while further details of the ensemble generation and the properties of the generated ensembles are described

in the Supplemental Material [27]. We discuss the results of the lattice form factors and the estimation of various sources of systematic uncertainties in Sec. IV. In Sec. V we discuss the continuum results for the form factors, the use of the  $z$ -parameter expansion to obtain results across the entire  $q^2$  range, and our main result: the determination of  $|V_{ub}|$  when our lattice form factors are combined with differential branching fractions from experiment. Finally, we conclude in Sec. VI.

## II. FORM FACTORS

Form factors to describe the semileptonic decay of a  $B$  meson to a pion can be defined for the transition matrix element  $\langle \pi(p_\pi) | V^\mu | B(p_B) \rangle$  of the flavor-changing vector current  $V^\mu = \bar{q} \gamma^\mu Q$  as

$$\langle \pi(p_\pi) | V^\mu | B(p_B) \rangle = f_+(q^2) \left[ p_B^\mu + p_\pi^\mu - \frac{M_B^2 - M_\pi^2}{q^2} q^\mu \right] + f_0(q^2) \frac{M_B^2 - M_\pi^2}{q^2} q^\mu, \quad (1)$$

where  $f_+(q^2)$  and  $f_0(q^2)$  are the vector and scalar form factors of this process,  $p_B$  and  $p_\pi$  are the four-momenta of the  $B$  and  $\pi$  respectively, and  $M_B$  and  $M_\pi$  are their masses. The momentum transfer is  $q^\mu = p_B^\mu - p_\pi^\mu$ . At  $q^2 = 0$  there exists a kinematic constraint,  $f_+(0) = f_0(0)$ .

A common alternative parametrization that is useful for lattice calculations relates the matrix elements to parallel and perpendicular form factors,  $f_\parallel(E_\pi)$  and  $f_\perp(E_\pi)$ , through

$$\langle \pi(p_\pi) | V^\mu | B(p_B) \rangle = \sqrt{2M_B} [v^\mu f_\parallel + p_{\pi,\perp}^\mu f_\perp], \quad (2)$$

where  $v^\mu = p_B^\mu / M_B$  is the velocity of the  $B$  meson, and  $p_{\pi,\perp}^\mu \equiv p_\pi^\mu - (v \cdot p_\pi) v^\mu$ . The pion energy  $E_\pi$  is related to the momentum transfer of the leptons by

$$E_\pi \equiv v \cdot p_\pi = \frac{M_B^2 + M_\pi^2 - q^2}{2M_B}. \quad (3)$$

Throughout this paper we keep the  $B$  meson on the lattice at rest and so can use the relations

$$f_\parallel(E_\pi) = \frac{\langle \pi(p_\pi) | V^0 | B(p_B) \rangle}{\sqrt{2M_B}}, \quad (4)$$

$$f_\perp(E_\pi) = \frac{\langle \pi(p_\pi) | V^i | B(p_B) \rangle}{\sqrt{2M_B}} \frac{1}{p_\pi^i}, \quad (5)$$

where the temporal,  $\mu = 0$ , and spatial,  $\mu = i$ , components of the vector current  $V^\mu$  are considered, respectively.

Another possible parametrization—motivated by heavy quark effective theory—is [28]

$$\langle \pi(p_\pi) | V^\mu | B(v) \rangle = 2 \left[ f_1(v \cdot p_\pi) v^\mu + f_2(v \cdot p_\pi) \frac{p_\pi^\mu}{v \cdot p_\pi} \right], \quad (6)$$

where the  $B$  meson state is defined as  $|B(v)\rangle = (1/\sqrt{M_B})|B(p_B)\rangle$  such that it is properly defined in the heavy quark limit. The form factors  $f_1(v \cdot p_\pi)$  and  $f_2(v \cdot p_\pi)$  are also consistently defined in the heavy quark limit and the heavy quark mass dependence would start from  $1/m_b$ . Comparing with Eqs. (4) and (5), we get

$$f_1(v \cdot p_\pi) + f_2(v \cdot p_\pi) = \frac{f_{\parallel}(E_\pi)}{\sqrt{2}}, \quad (7)$$

$$f_2(v \cdot p_\pi) = f_{\perp}(E_\pi) \left( \frac{v \cdot p_\pi}{\sqrt{2}} \right). \quad (8)$$

The relation to the conventionally defined form factors  $f_+(q^2)$  and  $f_0(q^2)$  is given by

$$f_+(q^2) = \sqrt{M_B} \left\{ \frac{f_2(v \cdot p_\pi)}{v \cdot p_\pi} + \frac{f_1(v \cdot p_\pi)}{M_B} \right\}, \quad (9)$$

$$f_0(q^2) = \frac{2}{\sqrt{M_B} M_B^2 - M_\pi^2} \left\{ [f_1(v \cdot p_\pi) + f_2(v \cdot p_\pi)] - \frac{v \cdot p_\pi}{M_B} \left[ f_1(v \cdot p_\pi) + \frac{M_\pi^2}{(v \cdot p_\pi)^2} f_2(v \cdot p_\pi) \right] \right\}, \quad (10)$$

or, equivalently, by

$$f_+(q^2) = \frac{1}{\sqrt{2} M_B} [f_{\parallel}(E_\pi) + (M_B - E_\pi) f_{\perp}(E_\pi)], \quad (11)$$

$$f_0(q^2) = \frac{\sqrt{2} M_B}{M_B^2 - M_\pi^2} [(M_B - E_\pi) f_{\parallel}(E_\pi) + (E_\pi^2 - M_\pi^2) f_{\perp}(E_\pi)]. \quad (12)$$

In the limit  $v \cdot p_\pi \rightarrow 0$ , the soft pion theorem and the pole dominance ansatz is justified using the heavy meson chiral Lagrangian approach and one obtains [28]

$$\lim_{v \cdot p_\pi \rightarrow 0} f_2(v \cdot p_\pi) = g_{B^* B \pi} \frac{f_{B^*} \sqrt{M_{B^*}}}{2 f_\pi} \frac{v \cdot p_\pi}{v \cdot p_\pi + \Delta_B}, \quad (13)$$

with  $M_{B^*}$  the mass of the vector meson  $B^*$ ,  $\Delta_B = M_{B^*} - M_B$  the hyperfine splitting,  $f_{B^*}$  and  $f_\pi$  the  $B^*$  and  $\pi$  decay constants respectively, and  $g_{B^* B \pi}$  the  $B^* B \pi$  coupling.

### III. LATTICE CALCULATION

#### A. Ensembles and correlators

We use the Möbius domain-wall fermion action [10] in this work for both heavy and light quarks. The gauge ensembles were generated with  $2 + 1$  flavors of dynamical quarks by the JLQCD Collaboration. The tree-level Symanzik-improved gauge action is employed, and stout smearing [29] is applied to the gauge fields when coupled to fermions. The lattice ensembles used in this work are

summarized in Table I. They form a subset of those generated by the JLQCD Collaboration. (The full list is found in the Supplemental Material [27].) Each ensemble is given an ID of the form “X-ud#-sa”, where X(=C, M, or F) denotes the lattice spacing, the number after  $ud$  represents the pion mass in units of 100 MeV, and the letter after  $s$  distinguishes whether the strange quark mass is above (a) or below (b) its physical value.

The simulation parameters are chosen as follows. The lattice spacings for coarse “C,” middle “M” and fine “F” lattices are 0.0804(1), 0.0547(1) and 0.0439(1) fm, corresponding to lattice cutoffs  $a^{-1} = 2.453(4)$ , 3.610(9) and 4.496(9) GeV, respectively. We use a range of light quark masses that correspond to pion masses from 500 MeV down to 230 MeV. They are roughly tuned to 500 ( $ud5$ ), 400 ( $ud4$ ), 300 ( $ud3$ ) and 230 ( $ud2$ ) MeV. Two values of strange quark mass are taken to sandwich its physical value on the coarsest lattice, i.e., above (sa) or below (sb) the physical strange quark mass. Lattice volumes are  $32^3 \times 64$ ,  $48^3 \times 96$  and  $64^3 \times 128$  for the three lattice spacings, respectively. They are chosen such that the spatial extent  $L$  of the lattice is kept constant,  $\sim 2.6$  fm, in physical units. The only exception is for the “C” ensemble with the lightest pion mass, “C-ud2-sa-L”, which has a larger volume of  $48^3 \times 96$ . The temporal extent  $N_T$  is chosen as  $N_T = 2L$ . All ensembles satisfy the condition  $M_\pi L > 4$ , which is often required to suppress the finite volume effects to a sufficient level, i.e., below a few per cent level for meson masses, decay constants, and form factors. We summarize the parameters of the gauge configurations including the light and strange sea quark masses,  $m_l$  and  $m_s$ , in Table I. The ID for each ensemble is the same as those in the Supplemental Material where further details about the lattice ensembles, including the measurement of the lattice spacing through the gradient flow, the observation of the topology tunnelings, and the light pseudoscalar meson masses and decay constants, are discussed [27].

The chiral symmetry of Möbius domain-wall fermions is not exact due to the finite fifth dimension  $L_5$ . The resulting residual mass depends on the lattice spacing and the details of the implementation of the domain-wall fermion. In our case the residual mass on the coarsest lattice ( $\beta = 4.17$ , the “C” lattices) is at the level of 1 MeV and an order of magnitude smaller on finer lattices (“M” and “F”). Detailed measurements are described in the Supplemental Material [27]. The residual mass, however, does not directly affect the analysis of the  $B \rightarrow \pi \ell \nu$  form factors because we use the pion and kaon masses as parameters to control the chiral extrapolation.

In addition to this work, the ensembles have so far been used for a determination of the renormalization constants [30], a calculation of the charmonium correlator and the extraction of the charm quark mass and the strong coupling constant [31], and a calculation of the  $D$  semileptonic decay form factors [32]. The lattice data have also been applied to

TABLE I. Parameters of the gauge configurations used in this analysis. We give the ID, the lattice spacing, coupling and dimensions in the first four columns. The number of configurations,  $N_{\text{cfg}}$ , are given in column five. We then provide the light, strange and heavy quark masses in lattice units in the next three columns respectively. Finally, we note the number of times sources  $N_{\text{tsrc}}$  used for each set of parameters, where a time source at  $t = 0$  is always employed, and additional time sources are evenly spaced in the time direction.

ID	$a$ (fm)	$\beta$	$L^3 \times N_T \times L_s$	$N_{\text{cfg}}$	$am_l$	$am_s$	$am_Q$	$N_{\text{tsrc}}$
C-ud5-sa	0.080	4.17	$32^3 \times 64 \times 12$	100	0.019	0.04	0.44037	2
							0.68808	2
C-ud5-sb	0.080	4.17	$32^3 \times 64 \times 12$	100	0.019	0.03	0.44037	2
							0.68808	1
C-ud4-sa	0.080	4.17	$32^3 \times 64 \times 12$	100	0.012	0.04	0.44037	2
							0.68808	2
C-ud4-sb	0.080	4.17	$32^3 \times 64 \times 12$	100	0.012	0.03	0.44037	2
							0.68808	1
C-ud3-sa	0.080	4.17	$32^3 \times 64 \times 12$	100	0.007	0.04	0.44037	4
							0.68808	4
C-ud3-sb	0.080	4.17	$32^3 \times 64 \times 12$	100	0.007	0.03	0.44037	4
							0.68808	1
C-ud2-sa-L	0.080	4.17	$48^3 \times 96 \times 12$	100	0.0035	0.04	0.44037	4
							0.68808	2
M-ud5-sa	0.055	4.35	$48^3 \times 96 \times 8$	50	0.012	0.025	0.27287	2
							0.42636	2
							0.68808	2
M-ud4-sa	0.055	4.35	$48^3 \times 96 \times 8$	50	0.008	0.025	0.27287	2
							0.42636	2
							0.68808	2
M-ud3-sa	0.055	4.35	$48^3 \times 96 \times 8$	42	0.0042	0.025	0.27287	4
							0.42636	2
							0.68808	2
F-ud3-sa	0.044	4.47	$64^3 \times 128 \times 8$	50	0.003	0.015	0.210476	4
							0.328869	2
							0.5138574	1

a calculation of the topological susceptibility in QCD [33], a study of the Dirac eigenvalue spectrum and a precise calculation of the chiral condensate [34], another study of the Dirac eigenvalue spectrum but in the high energy region [35], the short-distance current correlator and its comparison with experimental data [36], and a proposal for lattice calculations of inclusive  $B$  meson decays [25,26].

The valence sector also uses the Möbius domain-wall fermion action and the light quark masses are the same as used in the sea. Heavy quark masses were chosen as  $am_Q = 1.25^{2n} \times am_c$ , for  $n \geq 0$  and limited to values  $am_Q \leq 0.7$  to keep discretization errors under proper control. This results in mass values  $am_c \leq am_Q \leq 2.44 \times am_c$ . The charm quark mass in lattice units,  $am_c$ , is tuned such that the spin-averaged charmonium  $1S$  state reproduces its physical mass. (Details are discussed in Ref. [31].) Since the lowest heavy quark mass used is that of the charm, we have the process  $D \rightarrow \pi \ell \nu$  included as part of our dataset. We can then use form factors from that decay plus the additional heavier quark masses to extrapolate to the physical  $b$  quark mass.

In order to extract the form factors, we compute the three-point functions of the form

$$C_{3\text{pt}}^{\pi V^\mu B}(t, T) = \sum_{x,y,z} e^{i(p_\pi \cdot x + q \cdot y)} \langle P_\pi^S(x, 0) V^\mu(y, t) P_Q^S(z, T) \rangle, \quad (14)$$

where  $P_\pi^S$  and  $P_Q^S$  are interpolating operators to create or annihilate the pseudoscalar pion and heavy mesons. These operators are smeared to enhance the overlap with the corresponding ground state. The smearing is applied in a gauge invariant manner using an operator  $(1 - (\alpha/N)\Delta)^N$  with a discretized Laplacian  $\Delta$  and parameters  $\alpha = 20$  and  $N = 200$ . The source of the quark propagator is generated on the entire source time slice with random  $Z_2$  noise, and then the smearing is applied. The  $B$  meson is always set at rest so that  $\mathbf{q} = -\mathbf{p}_\pi$ . The source-sink separation in the temporal direction  $T$  is kept approximately fixed in physical units across all lattice spacings. We use  $T = 28, 42$  and  $56$  on ensembles with  $\beta = 4.17, 4.35$ , and  $4.47$ ,

respectively. The ground state can then be well isolated by the fits as described in Sec. III B.

The heavy-to-light vector current is defined as  $V^\mu = \bar{q}\gamma^\mu Q$ . Both light ( $q$ ) and heavy ( $Q$ ) quark fields are described by the Möbius domain-wall fermion action, and the current is local on the lattice. The renormalization constant  $Z_V$  is multiplied with the current afterwards, as discussed in Sec. III C.

We also compute the pion and heavy meson two-point functions. These are used to constrain the energies of the initial and final states in the combined fit, as discussed in Sec. III B.

These measurements are performed on  $N_{\text{cfg}}$  gauge configurations for each ensemble and repeated  $N_{\text{tsrc}}$  times by always using time source  $t = 0$  and then shifting the source and sink time slices by  $N_T/N_{\text{tsrc}}$ . The number of measurements is thus  $N_{\text{cfg}} \times N_{\text{tsrc}}$  per ensemble. Details are listed in Table I for each choice of ensemble and valence heavy quark mass.

## B. Two-point and three-point correlator fits

To extract the required form factors, we perform simultaneous fits of all two-point and three-point correlators for each set of ensembles and quark mass parameters using a constrained multiexponential fit [37]. Doing so allows us to fit the majority of the time extent of the correlators while isolating the ground states—needed to determine the form factors—from the excited states, which can be discarded. We include data starting from time slice  $t_{\text{min}} = 2, 3$  or 4 in the fit, depending on the ensemble. The two-point correlators are fit to the cosh form

$$C_P(t) = \sum_{n=0}^{n_{\text{exp}}-1} a_{P,n} b_{P,n}^* (e^{-E_{P,n}t} + e^{-E_{P,n}(N_T-t)}), \quad (15)$$

where the subscripts  $P, n$  correspond to state  $n$  of pseudoscalar  $P$ , such that  $n = 0$  is the ground state. The interpolating operators are always smeared at the source, and are either local or have the same smearing parameters at the sink. The amplitudes  $a_{P,n}$  and  $b_{P,n}$  are then equal for the smeared sink or different if the sink is local. We always fit both cases simultaneously to improve the determination of the ground-state energy. We use  $n_{\text{exp}} = 3$  and, since we only require ground-state energies and amplitudes for our calculation, we simply check that fits with two or four exponentials give consistent ground-state results. This multiexponential approach to our fits ensures the uncertainty due to contamination of excited states is taken into account.

For the three-point correlators, we fit to the form

$$C_{3\text{pt}}(t, T) = \sum_{n,m=0}^{n_{\text{exp}}-1} a_{\pi,n} V_{n,m} a_{B,m}^* e^{-E_{\pi,n}t} e^{-E_{B,m}(T-t)}. \quad (16)$$

The energies,  $E_{\pi,n}$  and  $E_{B,m}$ , and smeared amplitudes,  $a_{\pi,n}$  and  $a_{B,m}$ , are the same as those from the pion and heavy meson two-point correlator fit form. The amplitude  $V_{0,0}$ , which connects the ground-state heavy meson to the ground-state pion, is needed to determine the form factors. It relates to the corresponding matrix element by

$$V_{0,0}^\mu = \frac{\langle \pi | V^\mu | B \rangle}{2\sqrt{E_\pi M_B}}. \quad (17)$$

As with the two-point correlators, we use  $n_{\text{exp}} = 3$ .

We use the PYTHON packages GVAR [38], LSQFIT [39] and CORRFITTER [40] to fit our correlators. The fit parameters are given Bayesian priors as follows. The magnitudes of meson two-point amplitudes can be estimated by fitting that correlator alone with a single exponential at large time  $t$ , which leaves only the ground-state contribution. The heavy meson and pion two-point amplitudes are found to be of order 0.1–1.0 (smeared) and 10–30 (local), depending on the lattice spacing of the ensemble. These are taken as the central values, and the priors are given very conservative widths that are 5 times these values. Similarly, one can extract estimates of the magnitudes of the three-point amplitudes, which are found to be of order 1.0 ( $\mu = 0$ ) and 0.4 ( $\mu = 1, 2, 3$ ), and we again assign widths 5 times these values. Priors for the energies of ground states with zero momentum are given 10% widths. The energies of ground states with nonzero momentum get their priors according to the dispersion relation for energy using the prior of the zero momentum ground state. The gaps between energies of two consecutive states are given priors of  $\approx 0.7$  GeV with 70% widths.

We simultaneously fit a substantial amount of two-point and three-point correlator data, including multiple  $am_Q$  and  $q^2$  values. This can be difficult as we have to invert large covariance matrices in our fits. If the available statistics is limited, as it is in our case, the eigenvalues of the matrices tend to be underestimated and driven to zero. A standard way to deal with this is to impose singular value decomposition (svd) cuts  $c_{\text{svd}}$ . In this procedure any eigenvalue smaller than  $c_{\text{svd}}$  times the largest eigenvalue  $e_{\text{max}}$  is replaced by  $c_{\text{svd}}e_{\text{max}}$ . The use of the svd cuts makes the matrices less singular. This is a conservative approach since it can only serve to increase the final error. We have chosen the value of  $c_{\text{svd}}$  for each ensemble such that the fit quality is good while keeping as many eigenvalues as possible.

As we have to use fairly large svd cuts in these fits, using  $\chi^2$  per degree of freedom ( $\chi^2/N_{\text{dof}}$ ) as a measure of goodness-of-fit becomes less reliable. An svd cut increases the uncertainties in the data without increasing the random fluctuations in the data means. This tends to make the contributions from the parts of the  $\chi^2$  function affected by the svd cut much smaller than naively expected, which pulls  $\chi^2/N_{\text{dof}}$  down artificially. We therefore check the fits

and the final  $\chi^2/N_{\text{dof}}$  by adding extra noise to the priors and svd cut, which does not change the fits significantly.

In Figs. 1–6 we show how well our fit results agree with the correlator data for various values of lattice spacing, pion mass and heavy quark mass. In Fig. 1 (left panel) we plot a representative example of the ratio of three-point and two-point correlators,  $C_{V^0}(t)/(C_\pi(t)C_B(T-t))$ , alongside the fit result. The data at  $\beta = 4.17$ ,  $am_{u,d} = 0.007$  and  $am_Q = 0.44037$  with zero momentum insertion are shown. In the time range where the ground states dominate, this ratio will be a constant: the three-point ground-state amplitude divided by the two-point ground-state amplitudes. Towards  $T = 28$  we observe a significant curvature of the correlator ratio downward. If, on the other hand, we plot the ratio of the three-point correlator to the leading exponential functions  $e^{-E_\pi t}$  and  $e^{-M_B(T-t)}$ , a much longer plateau is evident as shown in Fig. 1 (right panel). This implies that the significant excited state contribution comes from the  $B$  meson two-point function. The plateau represents  $a_{\pi,0}V_{0,0}^\mu a_{B,0}^*$  in Eq. (16). In either case, the fit results

capture the excited-state effects in the data very well. We emphasize that we do not fit these correlator ratios. Rather, we use the simultaneous, multiexponential fits to two-point and three-point correlators described earlier in this section for each ensemble.

Similar plots of the three-point function divided by the ground-state exponentials are shown in Figs. 2–4 for the lattice data obtained at the coarsest lattice,  $\beta = 4.17$ . Here the data are shown for both temporal (left) and spatial (right) vector-current components for all available momentum insertions:  $(0,0,0)$ ,  $(0,0,1)$ ,  $(0,1,1)$ ,  $(1,1,1)$  in units of  $2\pi/L$ . Figures 2 and 3 should be compared for the effect of different light quark masses, while Figs. 2 and 4 should be compared for the effect of different heavy quark masses. In all cases, the fit results closely follow the lattice data.

The correlators computed on finer lattices are shown in Figs. 5 and 6. General observations are the same as those on the coarse lattice, but we observe larger noise due to limited statistics, especially on the finest lattice at  $\beta = 4.47$  (Fig. 6).

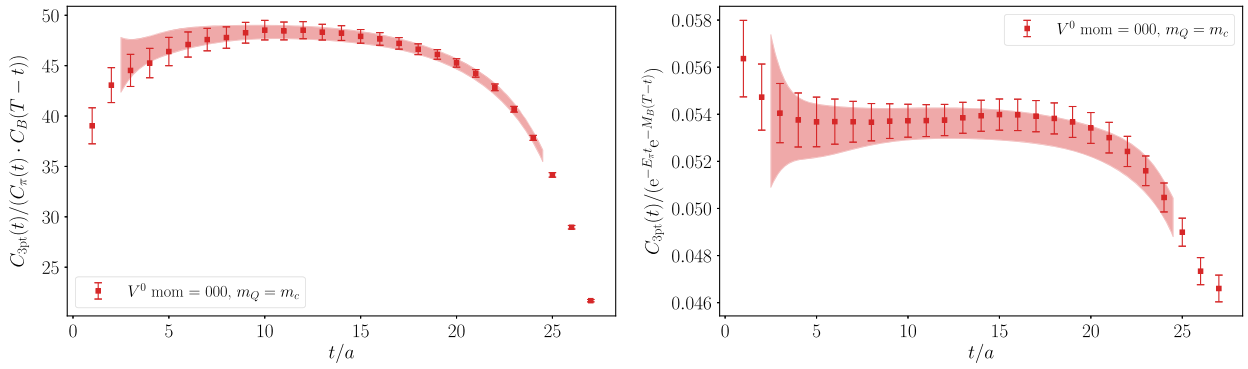


FIG. 1. Three-point correlator data with a  $V^0$  insertion on the ensemble with  $\beta = 4.17$ ,  $am_{u,d} = 0.007$  and  $am_Q = 0.44037$ . The bands represent the fit results and their fit range. The pion is created at  $t = 0$  while the  $B$  meson is annihilated at  $t = T$ . Left panel: the three-point correlator is divided by the pion and  $B$  meson two-point correlators. Right panel: the three-point correlator data is divided by the exponential function corresponding to the meson ground-state energies extracted from our fits.

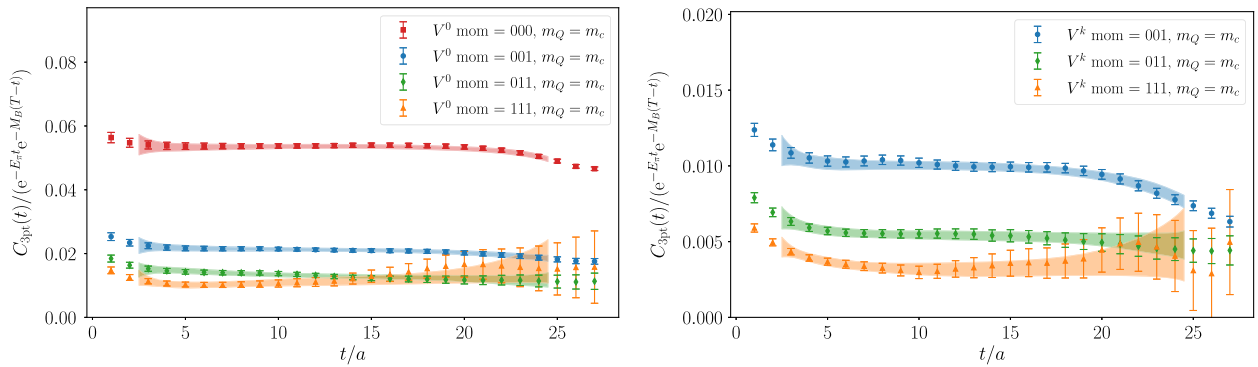
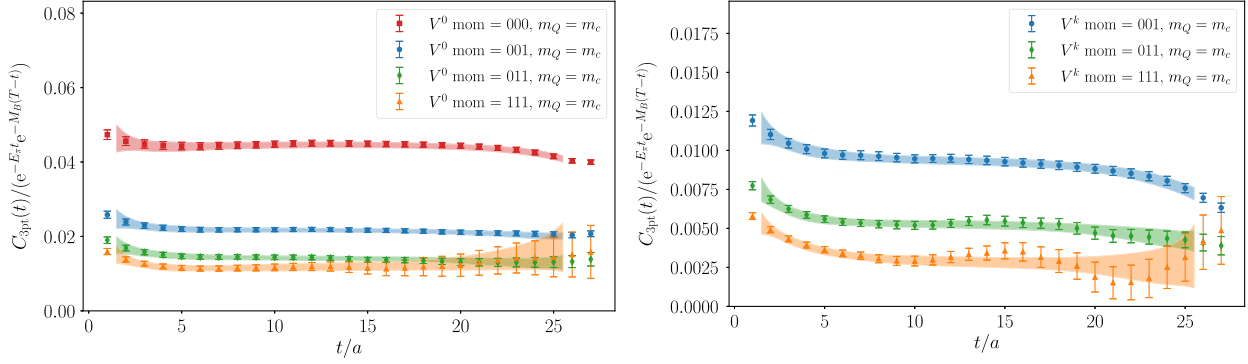
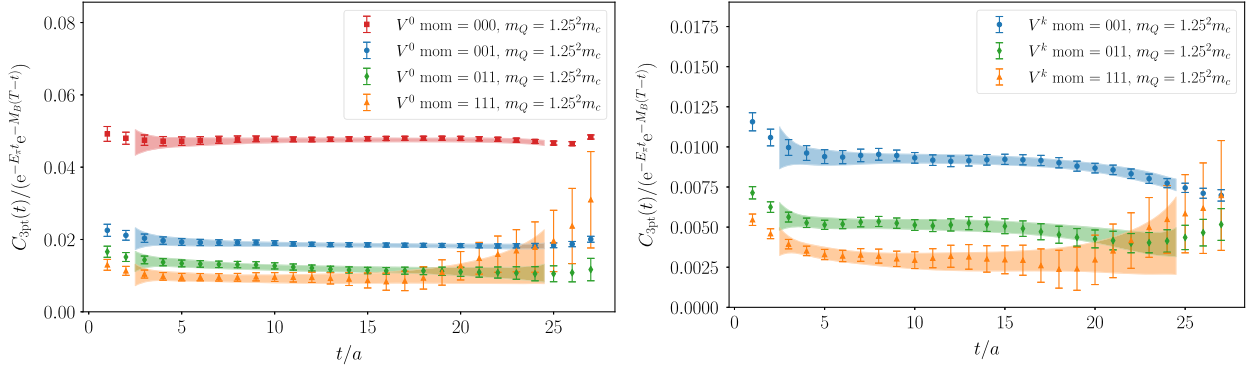
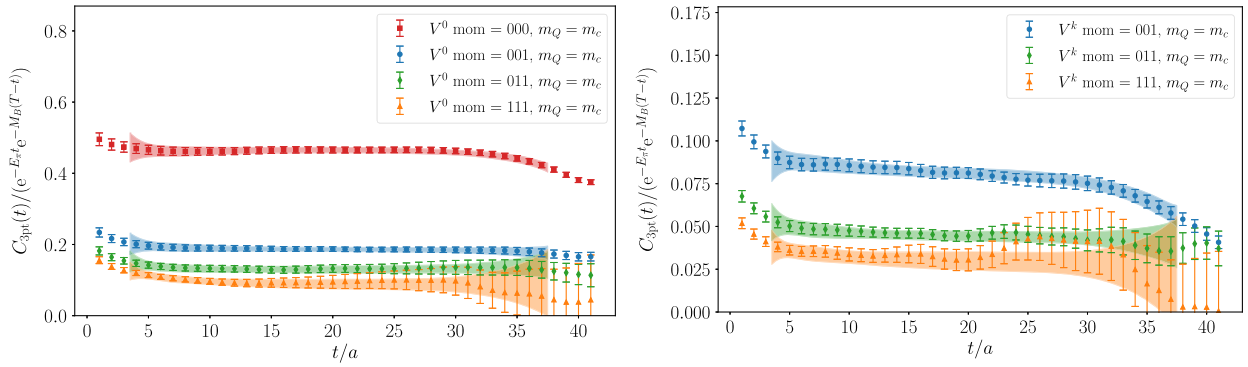
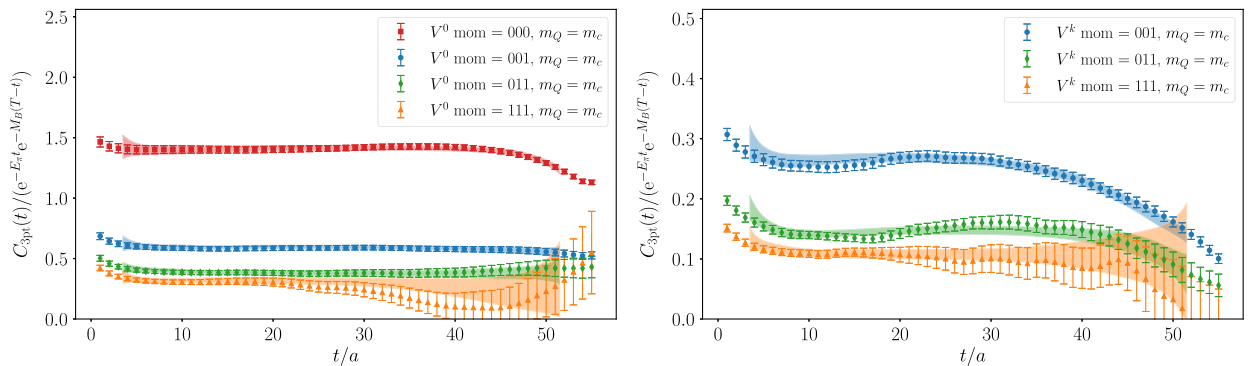


FIG. 2. Three-point correlators  $V^\mu$  divided by corresponding ground-state exponentials. Data is from the ensemble with  $\beta = 4.17$ ,  $am_{u,d} = 0.007$  and  $am_Q = 0.44037$ . The pion is created at  $t = 0$  while the  $B$  meson annihilated at  $t = T$ . Results for the temporal (left) and spatial (right) vector currents are shown for all available momenta:  $(0,0,0)$ ,  $(0,0,1)$ ,  $(0,1,1)$ ,  $(1,1,1)$  in units of  $2\pi/L$ .


 FIG. 3. Same as Fig. 2, but at heavier light quark mass  $am_{u,d} = 0.012$  while keeping the heavy quark mass as  $am_Q = 0.44037$ .

 FIG. 4. Same as Fig. 2, but at heavier heavy quark mass  $am_Q = 0.68808$  while keeping the light quark mass as  $am_{u,d} = 0.007$ .

 FIG. 5. Same as Fig. 2, but on a finer lattice,  $\beta = 4.35$ , and at  $am_{u,d} = 0.0042$  and  $am_Q = 0.27287$ .

 FIG. 6. Same as Fig. 2, but on the finest lattice,  $\beta = 4.47$ , and at  $am_{u,d} = 0.003$  and  $am_Q = 0.210476$ .

### C. Current renormalization

For the lightest heavy quark mass, i.e., when  $am_Q = am_c$ , we find that it is sufficient to renormalize our currents using results from the massless coordinate space current correlators as described in Ref. [36]. However, as discussed in Refs. [25,41], discretization effects arising from larger quark masses can lead to the renormalization constant  $Z_V$  from

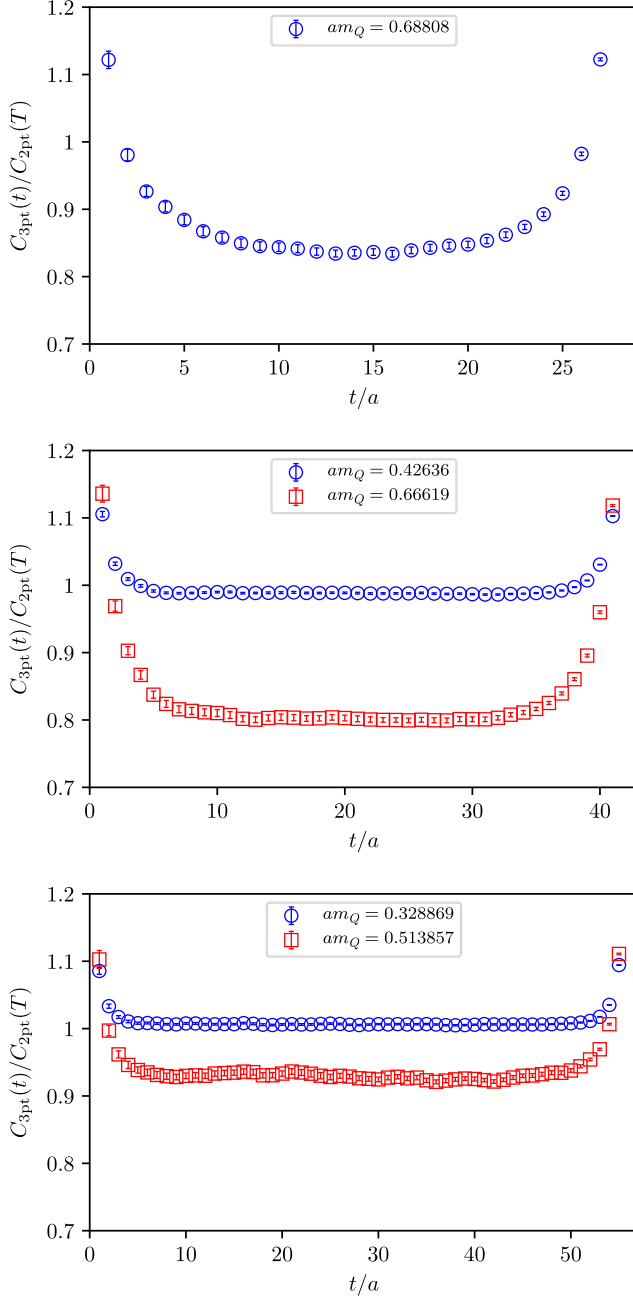


FIG. 7. Ratio of the  $B_s \rightarrow B_s$  three-point correlators at time slices  $t$  to the  $B_s$  two-point correlators. The data is from the ensembles with  $\beta = 4.17$  and  $am_l = 0.007$  (top),  $\beta = 4.35$  and  $am_l = 0.0042$  (middle), and  $\beta = 4.47$  (bottom). The heavy quark masses are shown in the plots. They correspond to  $m_Q = 1.25^2 m_c$  and  $1.25^4 m_c$ .

vector currents  $\bar{Q}\gamma_\mu Q$  deviating substantially from 1. We therefore consider it prudent to use the matrix element  $\langle B_s | \bar{Q}\gamma_\mu Q | B_s \rangle$  to partially renormalize our vector current alongside the massless renormalization results. (Here  $B_s$  stands for the pseudoscalar state comprising the heavy quark  $Q$  and the strange quark.)

By calculating three-point  $B_s \rightarrow B_s$  correlators and demanding that the inserted temporal vector current matrix element is 1—since it is conserved in the continuum—we can obtain the renormalization constant

$$Z_{V_{QQ}}^{-1} = \langle B_s | \bar{Q}\gamma_0 Q | B_s \rangle. \quad (18)$$

We then take the overall renormalization constant for the heavy-light current  $Z_V = \sqrt{Z_{V_{QQ}} Z_{V_{qq}}}$  where the renormalization constant for light-light current are determined as  $Z_{V_{qq}}^{-1} = 1.047(10)$ ,  $1.038(6)$ ,  $1.031(5)$  at  $\beta = 4.17$ ,  $4.35$ ,  $4.47$ , respectively [30].

We generated three-point correlators on each of the ensembles with the heavier of the available strange quark masses. On each ensemble and for each value of  $am_Q > am_c$  we used smeared sources and sinks with time separation  $T$ . We averaged over two time sources that were separated by half the temporal extent of the lattice. The exception was on the finest ensemble for which we used only a single time source. We also generated two-point correlators with the same sources so that we could extract the required matrix element by

$$\langle B_s | \bar{Q}\gamma_0 Q | B_s \rangle = \frac{C_{3\text{pt}}(t)}{C_{2\text{pt}}(T)}. \quad (19)$$

We show plots of the ratio from Eq. (19) in Fig. 7 for ensembles with  $\beta = 4.17$ ,  $4.35$  and  $4.47$ . We are able to find plateaus in all cases and thus simply fit to a constant in these regions. Table II gives the results for  $Z_{V_{QQ}}^{-1}$ .

TABLE II. Results for the inverse of the heavy-heavy renormalization constant  $Z_{V_{QQ}}^{-1}$  with statistical errors for each  $\beta$  value. In columns two and three we give the light and heavy quark masses respectively. We provide the fit ranges we used in column four.

$\beta$	$am_l$	$am_Q$	$[t_{\min}, t_{\max}]$	$Z_{V_{QQ}}^{-1}$	$\chi^2/N_{\text{dof}}$
4.17	0.019	0.68808	[11, 14]	0.8342(29)	0.45
	0.012	0.68808	[11, 14]	0.8382(35)	0.36
	0.007	0.68808	[11, 14]	0.8396(28)	0.46
4.35	0.012	0.42636	[8, 21]	0.9878(6)	0.38
		0.66619	[14, 21]	0.8013(24)	0.73
	0.008	0.42636	[8, 21]	0.9886(6)	0.83
		0.66619	[14, 21]	0.8031(27)	0.89
4.47	0.0042	0.42636	[8, 21]	0.9877(4)	0.73
		0.66619	[14, 21]	0.8020(26)	0.37
	0.003	0.328869	[12, 28]	1.0062(7)	0.96
	0.513857	[10, 28]	0.9267(14)	0.94	

## IV. RESULTS

### A. Global fit to form factors

In order to obtain the  $B$  to  $\pi$  form factors  $f_1(v \cdot p_\pi) + f_2(v \cdot p_\pi)$  and  $f_2(v \cdot p_\pi)$  at the physical quark masses and in the continuum limit, we perform a global fit. The form factors are functions of  $v \cdot p_\pi = E_\pi$ , which should also be parametrized. We assume the energy dependence of the form factor  $f_1(v \cdot p_\pi) + f_2(v \cdot p_\pi)$  is described by a simple polynomial, and use a fit function

$$f_1(v \cdot p_\pi) + f_2(v \cdot p_\pi) = C_0 \left( 1 + \sum_{n=1}^3 C_{E^n} N_E^n E_\pi^n \right) (1 + C_{\chi \log} \delta f^{B \rightarrow \pi} + C_{M_\pi^2} N_{M_\pi^2} M_\pi^2) \\ \times \left( 1 + \frac{C_{m_Q} N_{m_Q}}{m_Q} \right) (1 + C_{m_{s\bar{s}}^2} \delta m_{s\bar{s}}^2) (1 + C_{a^2} (\Lambda_{\text{QCD}} a)^2 + C_{(am_Q)^2} (am_Q)^2). \quad (20)$$

For  $f_2(v \cdot p_\pi)$ , since we expect a contribution from the vector meson ( $B^*$ ) pole as described in Eq. (13), we use

$$f_2(v \cdot p_\pi) = D_0 \left[ \frac{E_\pi}{E_\pi + \Delta_B} (1 + D_{E_\pi} N_E E_\pi) \right] (1 + D_{\chi \log} \delta f^{B \rightarrow \pi} + D_{M_\pi^2} N_{M_\pi^2} M_\pi^2) \\ \times \left( 1 + \frac{D_{m_Q} N_{m_Q}}{m_Q} \right) (1 + D_{m_{s\bar{s}}^2} \delta m_{s\bar{s}}^2) (1 + D_{a^2} (\Lambda_{\text{QCD}} a)^2 + D_{(am_Q)^2} (am_Q)^2). \quad (21)$$

Here  $C_x$  and  $D_x$  are fit parameters, and  $N_x$  are normalization constants that fix the units for energies and masses. These have been chosen so that  $C_x$  and  $D_x$  are  $\sim \mathcal{O}(1)$ . We choose  $N_E = 1/(0.3 \text{ GeV})$  and  $N_{M_\pi^2} = 1/(0.3 \text{ GeV})^2$ , where 0.3 GeV is a typical pion mass/energy, and  $N_{m_Q} = 1 \text{ GeV}^{-1}$ . We take  $\Lambda_{\text{QCD}} = 0.5 \text{ GeV}$ .

The heavy quark mass dependence as an expansion in terms of  $1/m_Q$  is justified because the form factors  $f_1(v \cdot p_\pi)$  and  $f_2(v \cdot p_\pi)$  can be defined even in the heavy quark limit. The  $1/m_Q$  term represents the first correction to that limit.

The strange quark masses have been set such that they are close to the physical strange quark mass. They are not, however, exactly tuned so we include the term

$$\delta m_{s\bar{s}}^2 = ((m_{s\bar{s}}^{\text{lat}})^2 - (m_{s\bar{s}}^{\text{phys}})^2) / (m_{s\bar{s}}^{\text{phys}})^2 \\ \equiv [(2(M_K^{\text{lat}})^2 - (M_\pi^{\text{lat}})^2) - (2(M_K^{\text{phys}})^2 - (M_\pi^{\text{phys}})^2)] / \\ [2(M_K^{\text{phys}})^2 - (M_\pi^{\text{phys}})^2] \quad (22)$$

in our fit to take this into account. Having two strange quark masses on either side of the physical mass on the coarsest lattice allows the fit to determine the coefficient of this correction term.

For the light quark mass dependence, we take the expectation from  $SU(2)$  ‘‘hard-pion’’ chiral perturbation theory for heavy-light mesons [42] (see also Ref. [43]):

$$\delta f^{B \rightarrow \pi} = -\frac{3}{4} (3g_{B^* B \pi}^2 + 1) \left( \frac{M_\pi}{4\pi f_\pi} \right)^2 \ln \frac{M_\pi^2}{\Lambda^2}, \quad (23)$$

plus a term linear in  $M_\pi^2$ . We take 1.0 GeV as the value for the scale  $\Lambda$  appearing in the chiral logarithm terms. For the pion decay constant  $f_\pi$  appearing in the denominator, we take  $f_\pi = 130.4 \text{ MeV}$ . The logarithmic dependence expected from chiral effective theory is not very significant with the precision of the current lattice data, and in our main fit we use the result from  $SU(2)$  chiral perturbation theory by fixing  $C_{\chi \log} = D_{\chi \log} = 1$ . However, this depends on the value we choose for the  $B^* B \pi$  coupling  $g_{B^* B \pi}$ . In the literature, the extracted values cover a wide range [44–49], and it is not straightforward to assess the overall uncertainty. On the other hand, it is not clear whether we can see the chiral log in our data. We therefore estimate the systematic uncertainty related to this term by setting  $g_{B^* B \pi} = 0.45$  [44] as a representative value in our main fit with fixed  $C_{\chi \log}$  and  $D_{\chi \log} = 1$ , followed by another fit where  $C_{\chi \log}$  and  $D_{\chi \log}$  are free fit parameters. In this way the uncertainty due to  $g_{B^* B \pi}$  is taken into account in the estimated systematic error. This is discussed in Sec. IV B.

We assume that the leading discretization effects appear as an overall factor of the form  $(1 + C_{a^2} (\Lambda_{\text{QCD}} a)^2 + C_{(am_Q)^2} (am_Q)^2)$ , and do not consider cross terms, e.g., a term of the form  $E_\pi a^2$  with independent parameters. This is justified because the dependence on the lattice spacing is small. We confirmed that adding such cross terms with free fit parameters has a negligible effect on the fit.

We find a good fit when simply fitting up to the quadratic term in pion energy for  $f_1(v \cdot p_\pi) + f_2(v \cdot p_\pi)$ , but larger uncertainties in data points with large pion momentum make it unclear what behavior is exhibited at higher pion energies. For this reason we include the cubic term in

TABLE III. Our best fit parameters from the global fit functions [Eqs. (20) and (21)].

$C_0$	$C_E$	$C_{E^2}$	$C_{E^3}$	$C_{M_\pi^2}$	$C_{m_Q}$	$C_{m_\pi^2}$	$C_{a^2}$	$C_{(am_Q)^2}$
1.33(8)	-0.37(5)	0.09(3)	-0.009(6)	0.096(10)	-0.34(6)	0.06(4)	-0.6(6)	0.04(7)
$D_0$	$D_E$	$D_{E^2}$	$D_{E^3}$	$D_{M_\pi^2}$	$D_{m_Q}$	$D_{m_\pi^2}$	$D_{a^2}$	$D_{(am_Q)^2}$
0.52(5)	-0.086(14)	...	...	0.026(15)	-0.09(14)	0.10(7)	0.03(1.09)	0.14(12)

Eq. (20). The impact of the choice to include this higher order term is minimal since, as we will discuss in Sec. VA, when extrapolating toward  $q^2 = 0$  we restrict our choice of synthetic data for the  $z$ -expansion to the region of pion energies covered by our simulation data. For  $f_2(v \cdot p_\pi)$  we only include a term linear in the pion energy.

Fitting both form factors  $f_1(v \cdot p_\pi) + f_2(v \cdot p_\pi)$  and  $f_2(v \cdot p_\pi)$  simultaneously, we obtain a fit with  $\chi^2/N_{\text{dof}} = 0.59$  ( $N_{\text{dof}} = 182$ ). We use Bayesian priors for the fit parameters: we choose  $1.0 \pm 2.0$  for  $C_0$  and  $D_0$ , and  $0.0 \pm 2.0$  for all other fit parameters. Results for the parameters from the global fit are given in Table III.

We illustrate the extrapolations in pion mass, heavy quark mass and lattice spacing in Figs. 8–10, respectively. Figure 8 shows the form factors  $f_1(v \cdot p_\pi) + f_2(v \cdot p_\pi)$  and  $f_2(v \cdot p_\pi)$  as functions of  $v \cdot p_\pi = E_\pi$  computed at different light quark masses corresponding to  $M_\pi = 300, 400$  and  $500$  MeV. The extrapolations to the chiral limit (or to the physical pion mass) are performed using the fit to Eqs. (20) and (21). One can see that the values of the form factors are rather stable as a function of the quark mass. The data points are well described by the global fit shown by

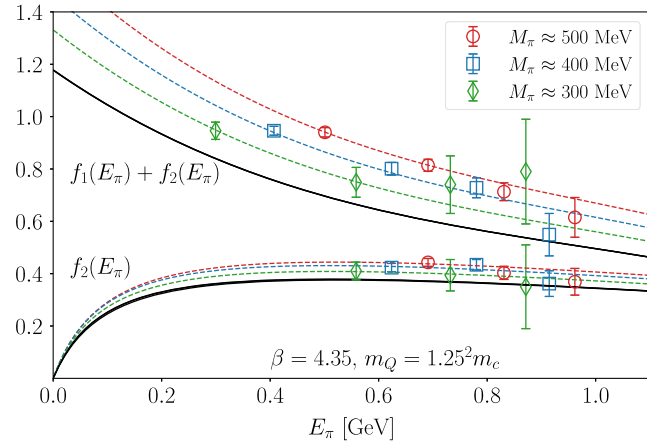


FIG. 8. Heavy-to-light form factors  $f_1(v \cdot p_\pi) + f_2(v \cdot p_\pi)$  and  $f_2(v \cdot p_\pi)$  at light quark masses corresponding to  $M_\pi \approx 300$  MeV (diamonds), 400 MeV (squares) and 500 MeV (circles). Data at  $\beta = 4.35$  ( $1/a \approx 3.6$  GeV) and at  $m_Q = 1.56m_c$ . Dashed curves are the results of the global fit at corresponding pion masses, and the solid curves show the fit results extrapolated to the physical pion mass.

dashed curves. The thick curves represent the results corresponding to the physical pion mass.

The heavy quark mass extrapolation is demonstrated in Fig. 9, which shows the form factors computed for three

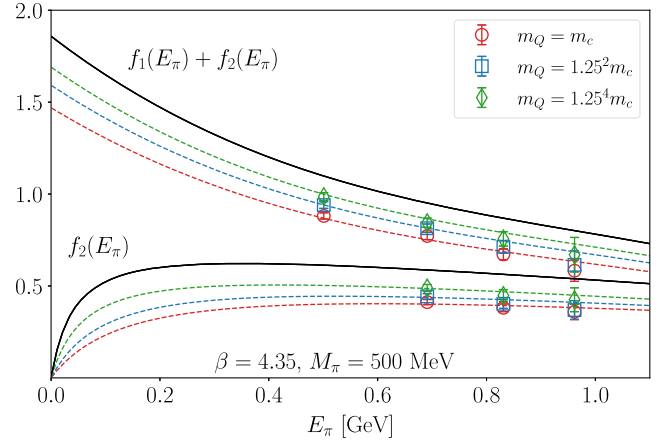


FIG. 9. Heavy-to-light form factors  $f_1(v \cdot p_\pi) + f_2(v \cdot p_\pi)$  and  $f_2(v \cdot p_\pi)$  at three different heavy quark masses:  $m_c$  (diamonds);  $1.56m_c$  (squares); and  $2.44m_c$  (circles). Data at  $\beta = 4.35$  ( $1/a \approx 3.6$  GeV) and at a fixed light quark mass corresponding to  $M_\pi \approx 500$  MeV. Dashed curves are the results of the global fit at corresponding heavy quark masses, and the solid curves show the fit results extrapolated to the physical  $b$  quark mass.

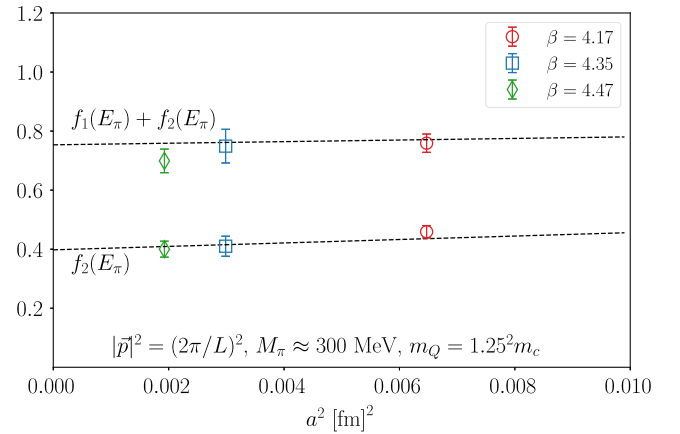


FIG. 10. Continuum extrapolation of the form factors  $f_1(v \cdot p_\pi) + f_2(v \cdot p_\pi)$  and  $f_2(v \cdot p_\pi)$  evaluated with a typical parameter choice:  $\mathbf{p}_\pi^2 = (2\pi/La)^2$  (note that the physical volumes of the three lattices are similar);  $M_\pi \approx 300$  MeV; and  $m_Q = 1.56m_c$ .

different heavy quark masses:  $m_Q = m_c$ ;  $1.56 \times m_c$ ; and  $2.44 \times m_c$ . We find that both form factors increase toward the physical  $b$  quark mass. As represented in Eqs. (20) and (21), we extrapolate assuming dependence of the form  $1/m_Q$ , and the results at the physical point are represented by the solid curves. The systematic error due to the effect of neglecting a  $1/m_Q^2$  term is estimated in the next subsection.

The continuum extrapolation is shown in Fig. 10 for a typical parameter choice ( $\mathbf{p}_\pi^2 = (2\pi/La)^2$ ,  $M_\pi \simeq 300$  MeV and  $m_Q = 1.56 \times m_c$ ). Since the physical volumes of the three lattices are similar, so too are the values of the physical momenta of the three points shown. We find that the continuum extrapolation in  $a^2$  is also mild, even though a potentially significant discretization effect due to the heavy quark mass of the form  $(am_Q)^2$  is expected. This is partly because the renormalization factor discussed in the previous section absorbs the bulk of the discretization effects. The global fit forms of Eqs. (20) and (21) assume that the discretization effect applies as an overall factor  $(1 + C_{a^2}(\Lambda_{\text{QCD}}a)^2 + C_{(am_Q)^2}(am_Q)^2)$ , independent of light quark masses and energies  $v \cdot p_\pi = E_\pi$ . This choice is justified because the dependence on each such parameter is small as we saw above. In principle this allows the global fit to discriminate between the  $(am_Q)^2$  and  $(\Lambda_{\text{QCD}}a)^2$  effects; in practice, both terms in our fits return coefficients consistent with zero.

The final results for  $f_1(v \cdot p_\pi) + f_2(v \cdot p_\pi)$  and  $f_2(v \cdot p_\pi)$  at the physical quark masses and in the continuum limit are shown in Fig. 11 as a function of  $v \cdot p_\pi = E_\pi$ . The bands represent the one standard deviation regions with only the statistical uncertainties included. The region that our lattice data cover is from 0.225 GeV to 0.975 GeV. The results outside of this region are obtained from the fit functions in Eqs. (20) and (21). In the soft pion limit, the form factor  $f_2(v \cdot p_\pi)$  rapidly goes to zero as a result of the pole term

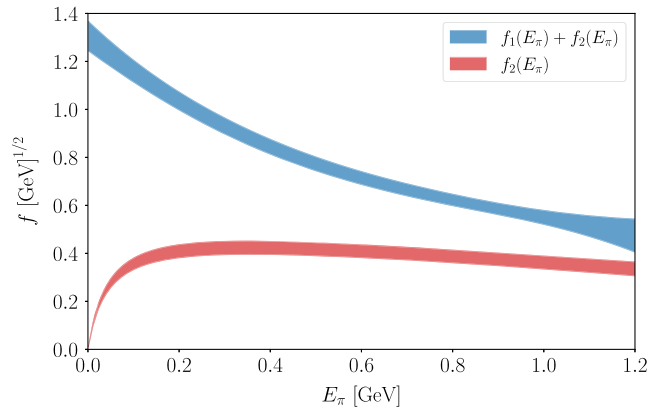


FIG. 11. Results of the global fit of the data for  $f_1(v \cdot p_\pi) + f_2(v \cdot p_\pi)$  (upper curve) to Eq. (20) and  $f_2(v \cdot p_\pi)$  (lower curve) to Eq. (21). The data from which these are obtained exist in the region  $0.225 \text{ GeV} < E_\pi < 0.975 \text{ GeV}$ .

included in Eq. (21), and is not directly confirmed by the lattice data.

## B. Estimation of systematic errors

We now turn to the analysis of systematic uncertainties. To make an assessment of their impact we perform additional fits with particular terms added or amended. We attempt the following variations of the fits:

- (1) The original fit using the form of Eqs. (20) and (21).
- (2) Adding a  $1/m_Q^2$  term such that the heavy quark dependence of  $f_1(v \cdot p_\pi) + f_2(v \cdot p_\pi)$  is parametrized by a factor  $(1 + C_{m_Q} N_{m_Q}/m_Q + C_{m_Q^2} N_{m_Q}^2/m_Q^2)$  instead of  $(1 + C_{m_Q} N_{m_Q}/m_Q)$ . Similarly for  $f_2(v \cdot p_\pi)$ .
- (3) Adding  $M_\pi^4$  terms such that the pion mass dependence of  $f_1(v \cdot p_\pi) + f_2(v \cdot p_\pi)$  is parametrized by a factor  $(1 + C_{\chi \log} \delta f^{B \rightarrow \pi}/(4\pi f_\pi)^2 + C_{M_\pi^2} N_{M_\pi^2} M_\pi^2 + C_{M_\pi^4} N_{M_\pi^4} M_\pi^4)$  instead of  $(1 + C_{\chi \log} \delta f^{B \rightarrow \pi}/(4\pi f_\pi)^2 + C_{M_\pi^2} N_{M_\pi^2} M_\pi^2)$ . Similarly for  $f_2(v \cdot p_\pi)$ .
- (4) Adding the next order term in  $E_\pi$ , so that  $f_1(v \cdot p_\pi) + f_2(v \cdot p_\pi)$  is parametrized by  $(1 + \sum_{n=1}^4 C_{E^n} N_{E^n} E_\pi^n)$  and  $f_2(v \cdot p_\pi)$  by  $(1 + \sum_{n=1}^2 D_{E^n} N_{E^n} E_\pi^n)$ .
- (5) Adding  $a^4$  terms such that the discretization effects of  $f_1(v \cdot p_\pi) + f_2(v \cdot p_\pi)$  are parametrized by a factor  $(1 + C_{a^2}(\Lambda_{\text{QCD}}a)^2 + C_{a^4}(\Lambda_{\text{QCD}}a)^4 + C_{(am_Q)^2}(am_Q)^2)$  instead of  $(1 + C_{a^2}(\Lambda_{\text{QCD}}a)^2 + C_{(am_Q)^2}(am_Q)^2)$ . Similarly for  $f_2(v \cdot p_\pi)$ .
- (6) Adding  $(am_Q)^4$  terms such that the discretization effects of  $f_1(v \cdot p_\pi) + f_2(v \cdot p_\pi)$  are parametrized by a factor  $(1 + C_{a^2}(\Lambda_{\text{QCD}}a)^2 + C_{(am_Q)^2}(am_Q)^2 + C_{(am_Q)^4}(am_Q)^4)$  instead of  $(1 + C_{a^2}(\Lambda_{\text{QCD}}a)^2 + C_{(am_Q)^2}(am_Q)^2)$ . Similarly for  $f_2(v \cdot p_\pi)$ .
- (7) Allowing the fit to determine the coefficient in front of the chiral log, i.e., letting  $C_{\chi \log}$  and  $D_{\chi \log}$  be free fit parameters instead of fixing them to 1.

We plot the result of these alternative fits in Fig. 12 at three representative  $q^2$  values ( $19.15 \text{ GeV}^2$ ,  $23.65 \text{ GeV}^2$  and  $26.40 \text{ GeV}^2$ ) after converting to  $f_0(q^2)$  and  $f_+(q^2)$ . The results are very stable across the alternative fits. The inner, lighter gray band shows our statistical uncertainty only, which is exactly the result from fit 1. The outer, darker gray band displays our total error, which includes systematic effects that come from the deviation from fit 1 of each of fits 2–7 added in quadrature.

We also plot the systematic uncertainty coming from each of the listed sources as a function of pion energy in Fig. 13 for both form factors  $f_0$  and  $f_+$ , covering the  $q^2$  range where we have data. They are estimated using the fits as described above, i.e., the deviation from the main fit “1” is plotted. They can therefore be either positive or negative. The estimated total systematic errors (red dash-dot lines), calculated from all sources of systematic uncertainty added in quadrature, are comparable in size to the statistical errors (blue solid lines).

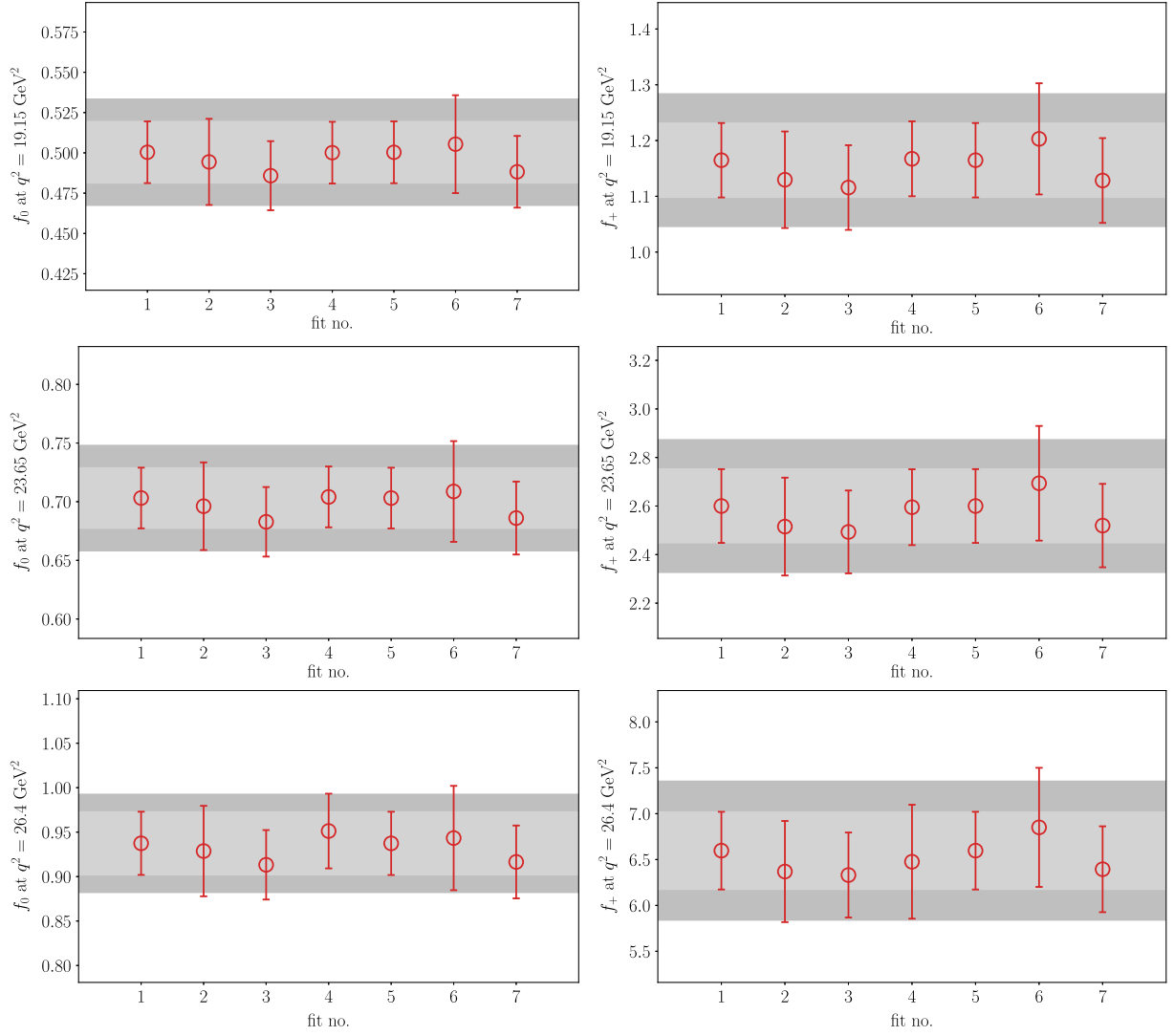


FIG. 12. Results for  $f_0(q^2)$  (left panels) and  $f_+(q^2)$  (right panels) for each of our fits (numbered according to the list in the text) in tests of systematic uncertainties. The results at representative values of  $q^2$  are shown: 19.15 GeV<sup>2</sup>, 23.65 GeV<sup>2</sup> and 26.40 GeV<sup>2</sup>. The inner gray bands are the statistical errors only, while the outer bands show the total statistical plus systematic uncertainties.

## V. FORM FACTORS IN THE CONTINUUM AND $|V_{ub}|$

The differential decay width relates to the form factors  $f_+(q^2)$  and  $f_0(q^2)$ , and  $|V_{ub}|$  through

$$\begin{aligned} \frac{d\Gamma(B \rightarrow \pi \ell \nu)}{dq^2} &= \frac{G_F^2 |V_{ub}|^2 (q^2 - m_\ell^2)^2 \sqrt{E_\pi^2 - M_\pi^2}}{24\pi^3 q^4 M_B^2} \\ &\times \left[ \left( 1 + \frac{m_\ell^2}{2q^2} \right) M_B^2 (E_\pi^2 - M_\pi^2) |f_+(q^2)|^2 \right. \\ &\left. + \frac{3m_\ell^2}{8q^2} (E_\pi^2 - M_\pi^2)^2 |f_0(q^2)|^2 \right], \quad (24) \end{aligned}$$

where  $G_F$  is Fermi's constant and  $m_\ell$  is the lepton mass. For electrons and muons the terms suppressed by  $m_\ell^2$  can be discarded (at least at the current theoretical and experimental

precision), which means that the contribution from the scalar form factor  $f_0$  can be neglected. Thus the relation between the differential decay width and the form factors is reduced to a much simpler form:

$$\frac{d\Gamma(B \rightarrow \pi \ell \nu)}{dq^2} = \frac{G_F^2 |V_{ub}|^2}{24\pi^3} |\mathbf{p}_\pi(q^2)|^3 |f_+(q^2)|^2, \quad (25)$$

where the pion momentum in the rest frame of the  $B$  meson is

$$|\mathbf{p}_\pi| = \frac{1}{2M_B} \sqrt{(M_B^2 + M_\pi^2 - q^2)^2 - 4M_B^2 M_\pi^2}. \quad (26)$$

To determine  $|V_{ub}|$ , we need the branching fractions obtained from experiment as well as form factors from our lattice calculation. In this section, we first discuss the parametrization of the  $q^2$  dependence of the form factors.

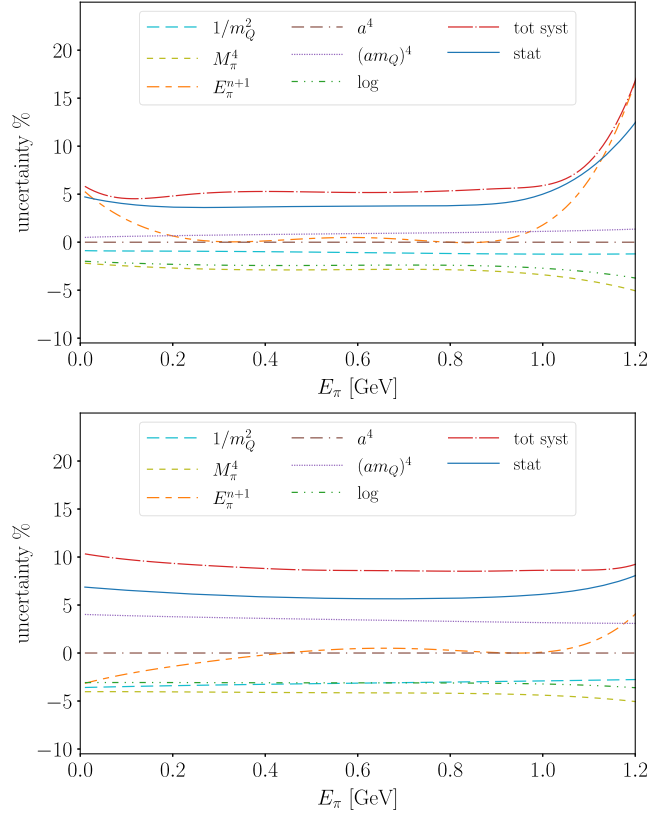


FIG. 13. Systematic errors as a function of pion energy for form factors,  $f_0$  (top panel) and  $f_+$  (bottom panel). Individual contributions are estimated using the fits as described in the text. The total systematic errors (red dash-dot lines) are obtained by adding the other systematic uncertainties in quadrature. The statistical errors are depicted by the blue solid lines.

The treatment of the experimental data is then described so that we can combine this with our lattice data to make a determination of  $|V_{ub}|$ .

### A. Form factor shape

We use the  $z$ -parameter expansion to parametrize the shape of the form factors. Here,  $q^2$  is transformed to a small parameter  $z$  as

$$z(q^2, t_0) = \frac{\sqrt{t_+ - q^2} - \sqrt{t_+ + t_0}}{\sqrt{t_+ - q^2} + \sqrt{t_+ + t_0}}, \quad (27)$$

where  $t_+ = (M_{B^0} + M_{\pi^+})^2$  is the  $B\pi$  threshold. We are free to choose the value of  $t_0 \leq t_+$ . We choose  $t_0 = (M_B + M_\pi)(\sqrt{M_B} - \sqrt{M_\pi})^2$  since this symmetrizes the values of  $z$  around 0, with  $|z| < 0.28$ .

For our final results of the  $f_+(q^2)$  form factor we fit our data to the Bourely-Caprini-Lellouch (BCL) expansion [18],

$$f_+(q^2) = \frac{1}{1 - q^2/M_{B^*}^2} \sum_{k=0}^{N_z-1} b_k^+ \left[ z^k - (-1)^{k-N_z} \frac{k}{N_z} z^{N_z} \right], \quad (28)$$

where the denominator on the right hand side addresses a pole at  $q^2 = M_{B^*}^2$ . The second term in parentheses is introduced to ensure that the form factor satisfies the appropriate asymptotic form near the threshold. For the scalar form factor,  $f_0(q^2)$ , we fit to a simple series expansion in  $z$ :

$$f_0(q^2) = \sum_{k=0}^{N_z-1} b_k^0 z^k. \quad (29)$$

Another widely used parametrization is the Boyd-Grinstein-Lebed (BGL) expansion [13,14]:

$$f_0(q^2) = \frac{1}{\mathcal{P}_0(q^2)\phi_0(q^2, t_0)} \sum_{n=0}^{N_z} a_n^0 z^n, \\ f_+(q^2) = \frac{1}{\mathcal{P}_+(q^2)\phi_+(q^2, t_0)} \sum_{n=0}^{N_z} a_n^+ z^n, \quad (30)$$

where  $\mathcal{P}_0(q^2)$  is usually taken as 1, and the pole in the vector form factor is taken care of by the Blaschke factor  $\mathcal{P}_+ = z(q^2, M_{B^*}^2)$ . The outer functions  $\phi_0(q^2, t_0)$  and  $\phi_+(q^2, t_0)$  are analytic. Often, the outer function for the scalar form factor is chosen as  $\phi_0(q^2, t_0) = 1$ . For the vector form factor we follow [50] and choose

$$\phi_+(q^2, t_0) = \sqrt{\frac{1}{32\pi\chi_J^{(0)}}} \left( \sqrt{t_+ - q^2} + \sqrt{t_+ - t_0} \right) \\ \times \left( \sqrt{t_+ - q^2} + \sqrt{t_+ - t_-} \right)^{3/2} \\ \times \left( \sqrt{t_+ - q^2} + \sqrt{t_+} \right)^{-5} \frac{(t_+ - q^2)}{(t_+ - t_0)^{1/4}}, \quad (31)$$

where  $t_\pm = (M_{B^0} \pm M_{\pi^+})^2$ ,  $t_0 = 0.65t_-$  and  $\chi_J^{(0)} = 6.9 \times 10^{-4} \text{ GeV}^{-2}$ . Note that the choice of  $t_0$  differs between the BCL and BGL  $z$ -expansion parametrizations in our analysis. Although our final results use the BCL parametrization, we confirmed that the BGL parametrization produces entirely consistent results.

The coefficients of the BCL ansatz in Eqs. (28) and (29) obey the unitarity constraint [18,51]

$$\sum_{m,n=0}^{N_z} B_{mn} b_m b_n \lesssim 1. \quad (32)$$

This holds for both  $b_k^+$  and  $b_k^0$ . The coefficients  $B_{mn}$  are symmetric in the indices,  $B_{mn} = B_{nm}$ , and satisfy the relation  $B_{mn} = B_{0|m-n|}$ . They depend on the choice of  $t_0$ ,

TABLE IV. Constants used to estimate the unitarity bound for the BCL ansatz, taken from Refs. [18,5].

	$B_{00}$	$B_{01}$	$B_{02}$	$B_{03}$	$B_{04}$	$B_{05}$
$f_0$	0.1032	0.0408	-0.0357	-0.0394	-0.0195	-0.0055
$f_+$	0.0198	0.0042	-0.0109	-0.0059	-0.0002	0.0012

and we list them for our choice  $t_0 = (M_B + M_\pi)(\sqrt{M_B} - \sqrt{M_\pi})^2$  for both form factors  $f_+$  and  $f_0$  in Table IV. We do not implement these constraints explicitly in our fits, but we do check that they are satisfied by our results.

From the results of the global fit, we generate synthetic data for a range of  $q^2$  values. Note that we have six degrees of freedom left after the extrapolations, so we can pick six data points (choosing more would result in a singular correlation matrix). We choose to generate three data points for each  $f_+(q^2)$  and  $f_0(q^2)$  at  $q^2$  values  $q_1^2 = 19.15$  GeV<sup>2</sup>,  $q_2^2 = 23.65$  GeV<sup>2</sup>, and  $q_3^2 = 26.40$  GeV<sup>2</sup>. We pick these so that they are approximately evenly spaced in  $z$ . The values of the form factors are given in Table V together with the statistical and systematic errors at each point. The correlation matrices of the statistical and systematic errors are provided in Table VI. The systematic covariance matrix is calculated as follows. For each reference  $q^2$  value, we first add all systematic effects listed in Sec. IV B in quadrature, including correlations between different effects. We can then calculate the (statistical) correlations between the total systematic effects (for both form factors  $f_+$  and  $f_0$ ) at different reference  $q^2$  values.

Our results for a fit to the BCL form of the  $z$ -expansion are given in Table VII. The correlation matrix of the resulting parameters  $b_k^+$  and  $b_k^0$  are in Table VIII. We do not use priors in this fit. We obtain a good fit when the order of the polynomial is chosen as  $N_z = 3$ . Here we impose the kinematic constraint  $f_+(0) = f_0(0)$ , i.e., we have six data points and five fit parameters. If we do not include the constraint then we have six data points and six fit parameters so cannot use  $\chi^2/N_{\text{dof}}$  as a measure of goodness of the fit. The fit result, however, remains unchanged. Although we do not impose them explicitly, we find that the unitarity constraints from Eq. (32) are satisfied and we get 0.034(16) and 0.122(44) for  $f_+$  and  $f_0$ , respectively.

TABLE V. Synthetic data points for  $f_+(q^2)$  and  $f_0(q^2)$  at  $q_1^2 = 19.15$  GeV<sup>2</sup>,  $q_2^2 = 23.65$  GeV<sup>2</sup>, and  $q_3^2 = 26.40$  GeV<sup>2</sup>. Their statistical and systematic errors are listed together with the total errors estimated by adding them in quadrature.

	$f_+(q_1^2)$	$f_+(q_2^2)$	$f_+(q_3^2)$	$f_0(q_1^2)$	$f_0(q_2^2)$	$f_0(q_3^2)$
Mean	1.165	2.600	6.597	0.500	0.703	0.937
Stat. err	0.067	0.152	0.423	0.019	0.026	0.036
Syst. err	0.099	0.229	0.631	0.027	0.037	0.043
Tot. err	0.120	0.275	0.760	0.033	0.045	0.056

TABLE VI. Statistical (upper panel) and systematic (lower panel) correlation matrix for the synthetic data points at  $q_1^2 = 19.15$  GeV<sup>2</sup>,  $q_2^2 = 23.65$  GeV<sup>2</sup>, and  $q_3^2 = 26.40$  GeV<sup>2</sup>.

	$f_+(q_1^2)$	$f_+(q_2^2)$	$f_+(q_3^2)$	$f_0(q_1^2)$	$f_0(q_2^2)$	$f_0(q_3^2)$
$f_+(q_1^2)$	1.000	0.957	0.901	0.799	0.728	0.663
$f_+(q_2^2)$	0.957	1.000	0.989	0.758	0.720	0.662
$f_+(q_3^2)$	0.901	0.989	1.000	0.708	0.682	0.639
$f_0(q_1^2)$	0.799	0.758	0.708	1.000	0.971	0.921
$f_0(q_2^2)$	0.728	0.720	0.682	0.971	1.000	0.943
$f_0(q_3^2)$	0.663	0.662	0.639	0.921	0.943	1.000

	$f_+(q_1^2)$	$f_+(q_2^2)$	$f_+(q_3^2)$	$f_0(q_1^2)$	$f_0(q_2^2)$	$f_0(q_3^2)$
$f_+(q_1^2)$	1.000	0.996	0.969	0.761	0.675	0.692
$f_+(q_2^2)$	0.996	1.000	0.981	0.737	0.650	0.663
$f_+(q_3^2)$	0.969	0.981	1.000	0.682	0.590	0.604
$f_0(q_1^2)$	0.761	0.737	0.682	1.000	0.992	0.996
$f_0(q_2^2)$	0.675	0.650	0.590	0.992	1.000	0.996
$f_0(q_3^2)$	0.692	0.663	0.604	0.996	0.996	1.000

We find that  $N_z = 2$  is insufficient for a good fit. We also test fitting the form factor  $f_+(q^2)$  alone using five synthetic data points. This makes very little difference to the  $f_+(q^2)$  results. We plot results of the form factors across the entire  $z$  range in Fig. 14. The blue squares show  $f_0$  and the red circles show  $(1 - q^2/M_{B^*}^2)f_+$ , while the bands are their corresponding fit results.

We can compare the form factors  $f_0(q^2)$  and  $f_+(q^2)$  to the results from other lattice QCD calculations when both statistical and systematic uncertainties are included. Results from the RBC and UKQCD Collaborations [4] and the Fermilab Lattice and MILC Collaborations [5] are plotted

TABLE VII. Fit results from the BCL  $z$ -expansion parametrization with  $N_z = 3$  on our synthetic lattice data. Coefficient  $b_0^0$  is fixed by the kinematic constraint  $f_+(0) = f_0(0)$ . The value is  $b_0^0 = 0.535(35)$ .

$b_0^+$	$b_1^+$	$b_2^+$	$b_1^0$	$b_2^0$
0.391(40)	-0.450(92)	-0.92(29)	-1.35(11)	0.33(31)

TABLE VIII. Correlation matrix from the  $z$ -expansion fit to our synthetic lattice data only with  $N_z = 3$  using the BCL parametrization. The constraint  $f_+(0) = f_0(0)$  has been applied (this determines  $b_0^0$ ).

	$b_0^+$	$b_1^+$	$b_2^+$	$b_1^0$	$b_2^0$
$b_0^+$	1.000	-0.515	-0.281	-0.100	0.102
$b_1^+$	-0.515	1.000	0.496	0.447	0.531
$b_2^+$	-0.281	0.496	1.000	0.606	0.790
$b_1^0$	-0.100	0.447	0.606	1.000	0.638
$b_2^0$	0.102	0.531	0.790	0.638	1.000

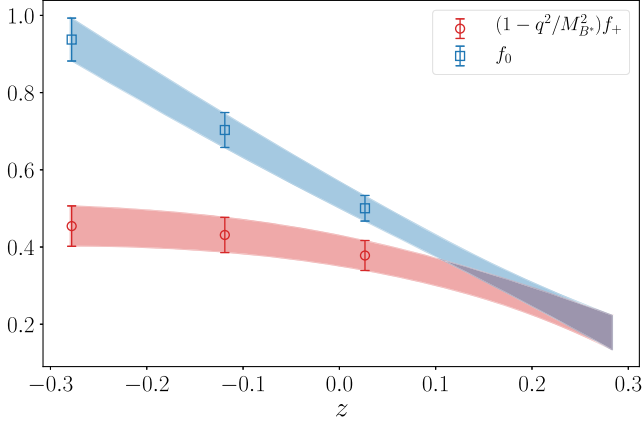


FIG. 14. Form factors using the BCL form of the  $z$ -parameter expansion. Lattice data for  $f_0$  (blue squares) and  $(1 - q^2/M_{B^*}^2)f_+$  (red circles) are shown with corresponding fit bands covering the entire  $z$  region.

alongside our results in Fig. 15. We restrict this comparison to the  $q^2$  region that approximately corresponds to the inserted pion momentum in the lattice calculations and find general agreement for both form factors. Near  $q_{\max}^2$  there are slight discrepancies with RBC/UKQCD for  $f_0(q^2)$  and Fermilab/MILC for  $f_+(q^2)$ . This may hint at some systematic effects, although the statistical significance is limited.

It is also interesting to compare the lattice form factors with theoretical expectations from heavy-quark symmetry. In the soft-pion limit, the vector and scalar form factors,  $f_+(q^2)$  and  $f_0(q^2)$ , are related by [28]

$$\lim_{q^2 \rightarrow M_b^2} \frac{f_0(q^2)}{f_+(q^2)} = \frac{f_B}{f_{B^*}} \frac{1 - q^2/M_{B^*}^2}{g_{B^*B\pi}}, \quad (33)$$

up to corrections of  $\mathcal{O}(1/m_b^2)$ . This ratio is plotted in Fig. 16 along with the theoretical expectation. We take

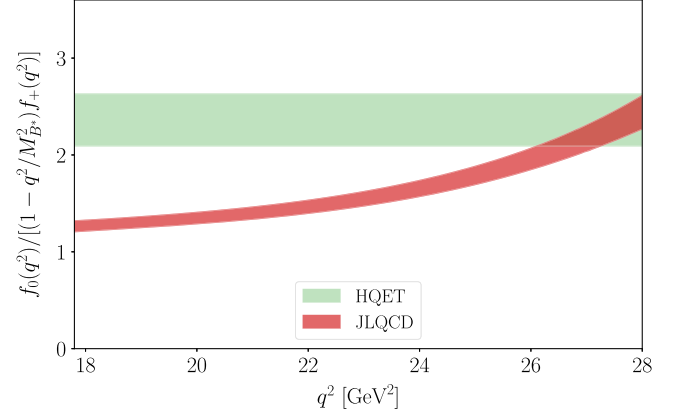
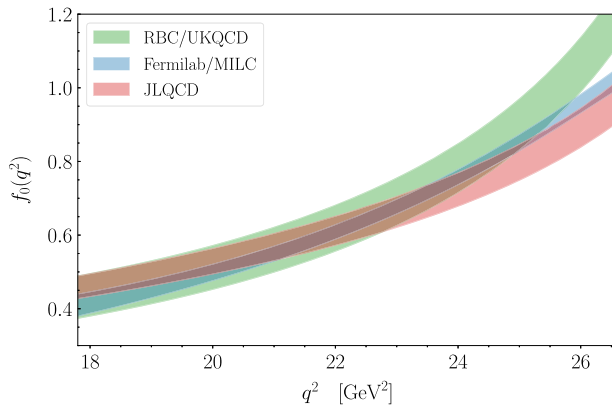


FIG. 16. Form factor ratio  $f_0(q^2)/[(1 - q^2/M_{B^*}^2)f_+(q^2)]$  as a function of  $q^2$  compared with the prediction in the soft-pion limit from heavy-quark symmetry and  $\chi$ PT [28]. The width of the green error band reflects only the uncertainties from  $g_{B^*B\pi} = 0.45(5)$  (from Ref. [44]) and  $f_{B^*}/f_B = 0.941(26)$  (from Ref. [52]), and not any other theoretical errors.

$g_{B^*B\pi} = 0.45(5)$  (from Ref. [44]) and  $f_{B^*}/f_B = 0.941(26)$  (from Ref. [52]). The width of the green error band that represents the heavy quark effective theory (HQET) expectation reflects only the uncertainties from  $g_{B^*B\pi}$  and  $f_{B^*}/f_B$ , and not any other theoretical errors. For the lattice data, we take our result of fit “1” extrapolated to the chiral limit  $M_\pi^2 = 0$ , showing only the statistical uncertainty. The agreement with the theoretical expectation in the soft pion limit and  $q^2 \rightarrow M_B^2$ , which is at the rightmost end of the plot, is excellent.

## B. Branching fractions from experiment

For the experimental results we use the following sets of data: the BABAR 2010 untagged analysis in 6 bins [50]; the Belle 2010 untagged analysis in 13 bins [53]; the BABAR 2012 untagged analysis in 12 bins [54]; and the Belle 2013 tagged analysis in which the  $B^0 \rightarrow \pi^+ \ell \nu$  process was

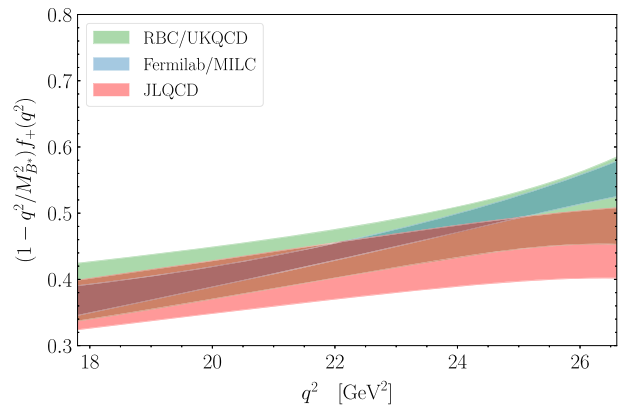


FIG. 15. Comparison of the physical form factors  $f_0(q^2)$  and  $f_+(q^2)$  with results from other lattice QCD calculations. Results from the RBC and UKQCD Collaborations are from Ref. [4] and results from the Fermilab Lattice and MILC Collaborations are from Ref. [5].

TABLE IX. Results of the fits to the branching fractions obtained from experiments.

Experiment	<i>BABAR</i> 2010	<i>BABAR</i> 2012	Belle 2010	Belle 2013	All	Excl. <i>BABAR</i> 2010
$b_1^+/b_0^+$	-0.85(47)	-0.24(44)	-1.25(26)	-1.79(51)	-0.96(19)	-1.05(21)
$b_2^+/b_0^+$	0.4(1.5)	-3.8(1.3)	-0.90(88)	1.1(1.6)	-1.37(60)	-1.42(65)
$b_0^+ V_{ub}  \times 10^3$	1.360(74)	1.499(59)	1.602(62)	1.558(85)	1.518(33)	1.557(36)
$\chi^2/N_{\text{dof}}$	1.99	0.45	1.18	1.26	1.39	1.07
<i>p</i> -value	0.11	0.91	0.30	0.21	0.04	0.36

measured in 13 bins and the  $B^- \rightarrow \pi^0 \ell \nu$  process was measured in 7 bins [55]. We deal with this last set of data by assuming isospin symmetry, which allows us to convert the  $B^-$  decay to the  $B^0$  decay through

$$\Delta\mathcal{B}(B^0 \rightarrow \pi^+ \ell \nu) = 2 \frac{\tau_{B^0}}{\tau_{B^-}} \Delta\mathcal{B}(B^- \rightarrow \pi^0 \ell \nu), \quad (34)$$

where the mean life of the neutral and charged  $B$  mesons are  $\tau_{B^0} = 1.519(4)$  ps and  $\tau_{B^-} = 1.638(4)$  ps, respectively [56]. These are the same sets of data as used by the Heavy Flavour Averaging Group (HFLAV) [20], the Flavour Lattice Averaging Group (FLAG) [21] and in the analysis presented in Ref. [57], as well as in the most recent lattice calculations of  $|V_{ub}|$  [4,5].

We assume that systematic correlations between each of the individual datasets are negligible. We do, however, include correlations from the systematic uncertainties in the Belle 2013 analysis between the 13-bin and 7-bin data. The Belle collaboration indicated systematic correlations of 49%. We construct a total covariance matrix for the  $B^0$  and  $B^-$  data (after conversion to the isospin symmetric  $B^0$  mode) by taking the direct sum of the statistical covariance matrices (where the off-diagonal blocks are  $\mathbf{0}$ ) and of the systematic covariance matrices (with 49% correlation between each of the bins in the off-diagonal blocks), and then summing these two  $20 \times 20$  matrices. The inclusion of these systematic correlations was found to have a negligible effect on the parameters and fit quality.

Our first step is fitting the four sets of data individually and then collectively without any lattice input. Using the BCL parametrization, we fit for the branching fraction in the  $i$ th bin through

$$\Delta\mathcal{B}_i = \frac{G_F^2 |V_{ub}|^2}{24\pi^3} \int_{q_i^2}^{q_{i+1}^2} |\mathbf{p}_\pi(q^2)|^3 |f_+(q^2)|^2 dq^2, \quad (35)$$

so that the combination of the form factor and CKM matrix element results in an overall normalization of  $b_0^+ |V_{ub}|$ .

The slope and the curvature from the  $z$ -expansion fits are captured in the ratios  $b_1^+/b_0^+$  and  $b_2^+/b_0^+$ , respectively. Table IX gives our results of fits to each of the branching fraction results with  $N_z = 3$ . We find that the fit quality is acceptable for each set of data when fitted individually, but that fitting all data simultaneously (“All”) results in a

relatively poor fit. This is due to a tension between the *BABAR* 2010 data and the other results. We confirm this by fitting various combinations of datasets, finding poor fit quality whenever *BABAR* 2010 is included. Therefore, we also give results for the case where *BABAR* 2010 is dropped (“Excl. *BABAR* 2010”), which results in an acceptable fit.

Fitting with  $N_z = 3$  is sufficient, and higher order fits do not improve the fit quality. Although we agree with the values of the fitted parameters for the *BABAR* 2012 data reported by the Fermilab Lattice and MILC Collaborations in Ref. [5], we find that the fit quality is actually better. Our result is in agreement with that found by the RBC and UKQCD Collaborations [4] and the result presented in Ref. [57] where they each find a similar discrepancy with the fit quality reported by the Fermilab Lattice and MILC Collaborations.

In Fig. 17 we plot 68% and 95% confidence regions for  $b_1^+/b_0^+$  and  $b_2^+/b_0^+$  for each of the cases listed in Table IX. This visually demonstrates the tension between the *BABAR* 2010 dataset and the other measurements. We also show the consistency between these shapes and with the shapes determined from our lattice fit to the form factors using the BCL parametrization with  $N_z = 3$  and with the kinematic constraint  $f_+(0) = f_0(0)$  imposed.

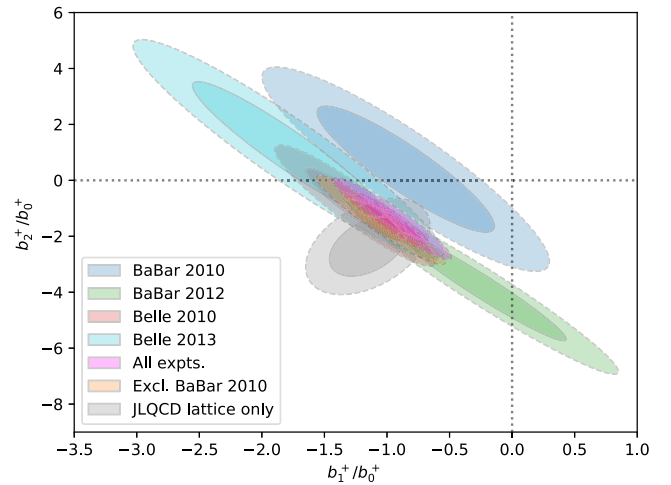


FIG. 17. Contour plots for the shape parameters  $b_1^+/b_0^+$  and  $b_2^+/b_0^+$ . We show 68% confidence regions with a solid outline, and 95% regions with a dashed outline.

### C. Determination of $|V_{ub}|$

We now turn to fitting the above branching fraction results alongside our form factor results from the lattice. In this way we can determine the  $z$ -expansion parameters  $b_n^+$  and our main result of  $|V_{ub}|$ , which appeared in the normalization of the experiment-only fits above. As discussed earlier, the contribution from the scalar form factor  $f_0(q^2)$  to the branching fraction is suppressed by the squared lepton mass, and we neglect it. Therefore only  $f_+(q^2)$  appears in Eq. (35). However, we do include lattice data for both form factors in the fit, and fit  $f_+(q^2)$ ,  $f_0(q^2)$  and experimental branching fraction data simultaneously. We impose the constraint  $f_+(0) = f_0(0)$  explicitly, although this makes a negligible difference to our final results since the low- $q^2$  region is primarily controlled by the branching fraction data.

As we have only three data points for  $f_0$ ,  $N_z = 4$  gives the maximum number of fit parameters we can use for  $f_0$  if the constraint  $f_+(0) = f_0(0)$  is imposed ( $N_z = 3$  without the constraint). For  $f_+$  we have data points from lattice and experiment, and are not limited to  $N_z = 4$ . We therefore choose  $(N_z^{f_+}, N_z^{f_0}) = (3, 3), (4, 4)$  and  $(5, 4)$  for our main fits (imposing the constraint at  $q^2 = 0$ ), and  $(N_z^{f_+}, N_z^{f_0}) = (3, 3), (4, 3)$  and  $(5, 3)$  for test fits without the constraint. We find that all these choices give a reasonable fit quality and the parameters are stable. We take  $(N_z^{f_+}, N_z^{f_0}) = (4, 4)$  for our accepted final result.

Numerical results for our combined lattice and experiment fits are given in Table X. We first fit the lattice form factors with each of the experimental branching fraction analyses in turn and find acceptable fit quality in each case. Next, we fit the lattice data alongside all experimental datasets simultaneously. As in the experiment-only fit, we do not find that the fit quality is particularly good when all experimental analyses are included. We therefore provide a

further set of numerical values for the case where the *BABAR* 2010 analysis is excluded. This improves the fit quality while all parameters are consistent with the all-experiment fit. It should be noted that when *BABAR* 2010 is excluded, the value of  $|V_{ub}|$  is determined to be marginally higher. The unitarity constraints from Eq. (32) are satisfied in each case, although we stress again that they are not explicitly imposed on the fits. The correlation matrices for the combined fit of all lattice and experimental data are in Table XI, while those without *BABAR* 2010 are in Table XII.

The differential branching fraction data from experiments, our lattice data (converted using  $|V_{ub}|$  from our accepted fit) and bands representing our  $z$ -expansion fit results with all errors included are plotted in Fig. 18. The differences among the results with different  $(N_z^{f_+}, N_z^{f_0})$  are hardly visible, and they give essentially the same result for  $|V_{ub}|$ . We reiterate that we take  $(N_z^{f_+}, N_z^{f_0}) = (4, 4)$  as our main result. In Fig. 19 we again show the form factors across the entire  $z$  range, this time using the above BCL fits combining lattice form factor data and branching fractions from experiment. The lattice data for  $f_0$  (blue squares) and  $(1 - q^2/M_{B^*}^2)f_+$  (red circles) are shown with corresponding fit bands from the combined fit.

Our final result for  $|V_{ub}|$  is thus from the combined fit with all experimental data:

$$|V_{ub}| = (3.93 \pm 0.41) \times 10^{-3}. \quad (36)$$

The uncertainty includes the statistical and systematic errors originating from our lattice calculation as well as the total errors from the experimental data. If we exclude the *BABAR* 2010 dataset from the analysis, we obtain  $|V_{ub}| = (4.01 \pm 0.42) \times 10^{-3}$  with a much improved  $p$ -value (see Table X).

Our result for  $|V_{ub}|$  is compared with other lattice QCD calculations and exclusive and inclusive determinations by

TABLE X. Results of the simultaneous fits to form factors from our lattice calculation and experimental branching fractions, with  $(N_z^{f_+}, N_z^{f_0}) = (4, 4)$ . We list  $b_0^0$  here for completeness, but it is fixed through the constraint  $f_+(0) = f_0(0)$ .

Experiment	<i>BABAR</i> 2010	<i>BABAR</i> 2012	Belle 2010	Belle 2013	All	Excl. <i>BABAR</i> 2010
$b_0^+$	0.388(40)	0.385(40)	0.390(40)	0.388(40)	0.389(40)	0.390(40)
$b_1^+$	-0.389(80)	-0.350(78)	-0.438(76)	-0.469(84)	-0.391(66)	-0.411(69)
$b_2^+$	-0.20(18)	-0.72(16)	-0.66(16)	-0.57(18)	-0.62(15)	-0.66(15)
$b_3^+$	1.79(77)	-0.40(64)	0.23(65)	0.96(76)	0.22(52)	0.09(5)
$b_0^0$	0.535(35)	0.536(35)	0.535(35)	0.533(35)	0.536(35)	0.536(35)
$b_1^0$	-1.31(12)	-1.33(12)	-1.35(12)	-1.35(12)	-1.33(12)	-1.34(12)
$b_2^0$	1.16(23)	0.56(17)	0.59(17)	0.71(21)	0.68(16)	0.60(16)
$b_3^0$	2.4(1.1)	0.63(97)	0.88(98)	1.3(1.0)	1.03(96)	0.85(96)
$ V_{ub}  \times 10^3$	3.58(41)	4.04(43)	4.10(45)	3.91(45)	3.93(41)	4.01(42)
$\sum B_{mn}^+ b_m^+ b_n^+$	0.075(59)	0.027(14)	0.023(9)	0.038(31)	0.020(8)	0.022(7)
$\sum B_{mn}^0 b_m^0 b_n^0$	1.07(70)	0.21(24)	0.28(29)	0.44(42)	0.32(32)	0.27(28)
$\chi^2/N_{\text{dof}}$	1.43	0.77	1.13	1.22	1.37	1.05
$p$ -value	0.22	0.66	0.33	0.23	0.04	0.38

TABLE XI. Correlation matrix from the  $z$ -expansion fit to all experiments and our synthetic lattice data with  $(N_z^{f_+}, N_z^{f_0}) = (4, 4)$  parameters. Note that  $b_0^0$  is fixed by the constraint  $f_+(0) = f_0(0)$ .

	$ V_{ub} $	$b_0^+$	$b_1^+$	$b_2^+$	$b_3^+$	$b_1^0$	$b_2^0$	$b_3^0$
$ V_{ub} $	1.000	-0.980	0.568	0.346	0.007	0.051	-0.409	-0.060
$b_0^+$	-0.980	1.000	-0.652	-0.379	0.048	-0.067	0.392	0.064
$b_1^+$	0.568	-0.652	1.000	-0.024	-0.570	0.093	-0.349	-0.159
$b_2^+$	0.346	-0.379	-0.024	1.000	-0.192	0.153	0.066	-0.050
$b_3^+$	0.007	0.048	-0.570	-0.192	1.000	-0.158	0.126	0.251
$b_1^0$	0.051	-0.067	0.093	0.153	-0.158	1.000	0.388	-0.647
$b_2^0$	-0.409	0.392	-0.349	0.066	0.126	0.388	1.000	-0.376
$b_3^0$	-0.060	0.064	-0.159	-0.050	0.251	-0.647	-0.376	1.000

TABLE XII. Correlation matrix from the  $z$ -expansion fit of our synthetic lattice data and experiment excluding BABAR 2010 with  $(N_z^{f_+}, N_z^{f_0}) = (4, 4)$  parameters. Note that  $b_0^0$  is fixed by the constraint  $f_+(0) = f_0(0)$ .

	$ V_{ub} $	$b_0^+$	$b_1^+$	$b_2^+$	$b_3^+$	$b_1^0$	$b_2^0$	$b_3^0$
$ V_{ub} $	1.000	-0.977	0.552	0.379	0.039	0.056	-0.367	-0.040
$b_0^+$	-0.977	1.000	-0.643	-0.412	0.019	-0.073	0.348	0.045
$b_1^+$	0.552	-0.643	1.000	-0.008	-0.573	0.102	-0.326	-0.157
$b_2^+$	0.379	-0.412	-0.008	1.000	-0.141	0.153	0.079	-0.035
$b_3^+$	0.039	0.019	-0.573	-0.141	1.000	-0.159	0.132	0.260
$b_1^0$	0.056	-0.073	0.102	0.153	-0.159	1.000	0.393	-0.646
$b_2^0$	-0.367	0.348	-0.326	0.079	0.132	0.393	1.000	-0.382
$b_3^0$	-0.040	0.045	-0.157	-0.035	0.260	-0.646	-0.382	1.000

HFLAV and FLAG in Fig. 20. Compared with other lattice QCD computations of the  $B \rightarrow \pi \ell \nu$  process (Fermilab/MILC [5], RBC/UKQCD [4] and HPQCD [3]) our result is slightly higher but still consistent within the estimated

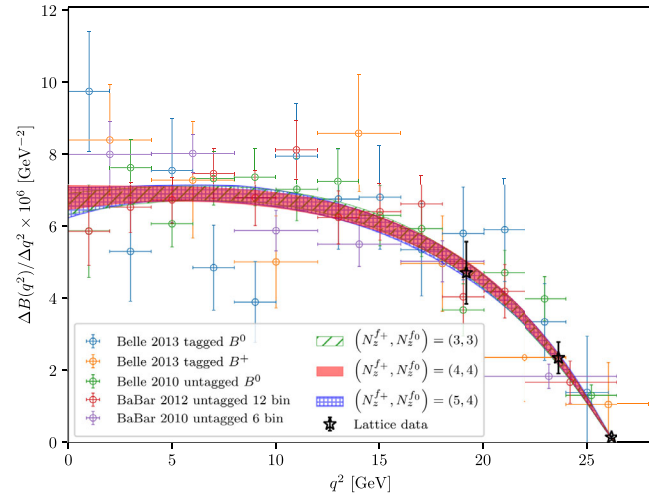


FIG. 18. Fitting experimental branching fractions together with form factors from lattice QCD to extract  $|V_{ub}|$ . The error bands show our fit results when we include  $(N_z^{f_+}, N_z^{f_0})$  terms in the  $z$ -expansion. We find that  $N_z^{f_+} \geq 3$  gives a reasonable fit quality, and take  $(N_z^{f_+}, N_z^{f_0}) = (4, 4)$  as our main result.

errors. Our result is also compatible with the inclusive determination, which we have taken from HFLAV [20] using the “GGOU” analysis. We include dashed error bars to indicate the spread of results from other methods. We also note that our value is in good agreement with those of Refs. [57–59], while moderately higher than—but still

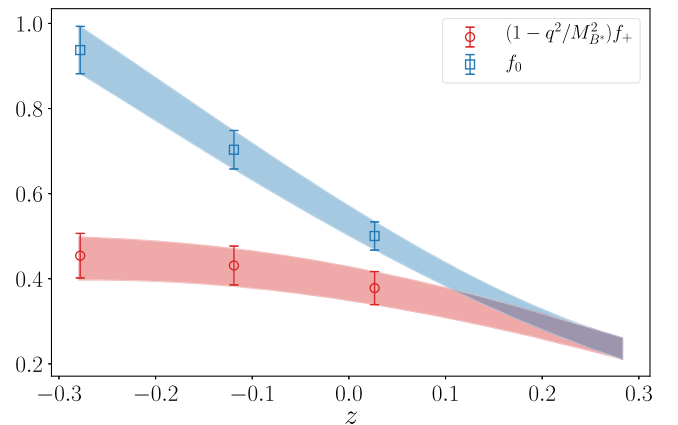


FIG. 19. Form factors using the BCL form of the  $z$ -parameter expansion determined from a combined fit of lattice data and branching fractions from experiment. Lattice data for  $f_0$  (blue squares) and  $(1 - q^2/M_{B^*}^2)f_+$  (red circles) are shown with fit bands covering the entire  $z$  region.

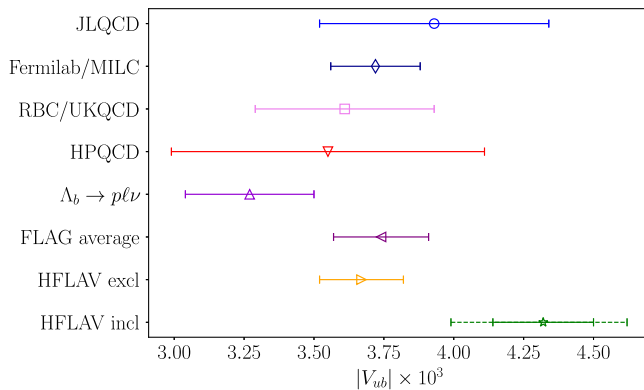


FIG. 20. Comparison of our result for  $|V_{ub}|$  with other lattice QCD calculations and exclusive and inclusive determinations by HFLAV and FLAG. The data point labeled “JLQCD” is our final result (this work). Other results are from the following publications: the Fermilab Lattice and MILC Collaborations [5]; the RBC and UKQCD Collaborations [4]; and the HPQCD Collaboration [3]. The value tagged  $\Lambda_b \rightarrow p \ell \nu$  is from Refs. [61,62]. This combines a lattice QCD calculation of the form factors of the  $\Lambda_b$  to  $p$  process with experimental measurement of the ratio  $\mathcal{B}(\Lambda_b^0 \rightarrow p \mu^- \bar{\nu}_\mu) / \mathcal{B}(\Lambda_b^0 \rightarrow \Lambda_c^+ \mu^- \bar{\nu}_\mu)$  presented by the LHCb Collaboration, which allows the extraction of the ratio  $|V_{ub}|/|V_{cb}|$ . Using  $|V_{cb}| = (39.5 \pm 0.8) \times 10^{-3}$  from exclusive decays [62,63], the authors quoted a value for  $|V_{ub}|$ . The FLAG average is from the 2021 report [21], and the HFLAV exclusive and inclusive results are from Ref. [20]. The inclusive data point is from their GGOU analysis, with a second (dashed) error bar to represent the spread of values from other frameworks.

consistent with—that in Ref. [60], all of which use lattice form factor results as input.

## VI. CONCLUSIONS

For the determination of  $|V_{ub}|$ , the combination of the lattice computation of form factors and the experimental measurements of the differential cross section is crucial. This is not solely because the experiments can only measure the product of the form factor  $f_+(q^2)$  and  $|V_{ub}|$ , but because they provide complementary information about the form factor shape. The lattice calculation provides the form factor in the large  $q^2$  region with controlled errors, while the experimental data are more sensitive to the low  $q^2$  region. As one can see from the fit results, by combining the data from both experiment and lattice QCD, the form factor shape is much better controlled.

Our combined result for  $|V_{ub}|$  is  $3.93(41) \times 10^{-3}$  when including data from all experiments, and  $4.01(42) \times 10^{-3}$  when excluding the 6-bin untagged *BABAR* 2010 analysis. In both cases these results are consistent with the inclusive determination of  $|V_{ub}|$  and with previous results on the exclusive  $B \rightarrow \pi \ell \nu$  process.

The advantage of our lattice calculation over previous work is the use of a fully relativistic lattice fermion

formulation, with which no extra matching procedure is required. (For the renormalization constant, we employed a strategy to eliminate the bulk of the large discretization effects appearing in the wave-function renormalization by making a non-perturbative determination of  $Z_V$  using heavy-to-heavy three-point functions.) Our analysis therefore becomes rather straightforward: we simply assume the discretization effects are of  $\mathcal{O}(a^2)$  and  $\mathcal{O}((am_Q)^2)$  and let the numerical data determine their size by combining the lattice data at various  $a$  and  $am_Q$ . We also explore the dependence on the heavy quark mass and find that it is consistent with a leading  $1/m_Q$  correction to the heavy quark limit.

A major challenge in this analysis was due to the multiple extrapolations that have to be performed at the same time in three parameter dimensions: the light quark mass; the heavy quark mass; and the lattice spacing. We find that these limits are reached rather smoothly with our global fit function. We estimate systematic errors due to potentially missing higher order terms in the ansatz by attempting the fit including one such term at a time. There is no single dominant source of error, but after adding them in quadrature the total systematic error is comparable to the statistical error in our calculation. The inclusion of heavier masses for  $m_Q$  and smaller pion masses would help further control systematic effects, while additional statistics is the key to improving the calculation of these form factors in the future.

We anticipate more lattice calculations of the  $B \rightarrow \pi \ell \nu$  process using fully relativistic actions in the near future. Crucially, this includes cases where the heavy quark is tuned to the physical  $b$  quark mass on the finest lattices, allowing for an improved approach to the physical point, and therefore even better control of systematic effects.

## ACKNOWLEDGMENTS

We would like to thank Zechariah Gelzer and Justus Tobias Tsang for useful discussions during this project. We also thank members of the JLQCD Collaboration for discussions and for providing the computational framework. In particular, we are grateful to Brendan Fahy for his participation in the early stage of this work, and to Guido Cossu and Jun-Ichi Noaki for the development of the IroIro++ code set [64], which was used to generate the data. Numerical calculations were performed on the Blue Gene/Q supercomputer at KEK under its Large Scale Simulation Program (No. 16/17-14). This work is supported in part by JSPS KAKENHI Grants No. 18H03710 and No. 21H01085, and by MEXT as “Program for Promoting Researches on the Supercomputer Fugaku” (Simulation for basic science: from fundamental laws of particles to creation of nuclei, JPMXP1020200105) through the Joint Institute for Computational Fundamental Science (JICFuS). The reference list was automatically populated using *filltex* [65].

- [1] B. Colquhoun, R. J. Dowdall, J. Koponen, C. T. H. Davies, and G. P. Lepage, *Phys. Rev. D* **93**, 034502 (2016).
- [2] C. Hughes, C. T. H. Davies, and C. J. Monahan, *Phys. Rev. D* **97**, 054509 (2018).
- [3] E. Dalgic, A. Gray, M. Wingate, C. T. H. Davies, G. P. Lepage, and J. Shigemitsu, *Phys. Rev. D* **73**, 074502 (2006); **75**, 119906(E) (2007).
- [4] J. M. Flynn, T. Izubuchi, T. Kawanai, C. Lehner, A. Soni, R. S. Van de Water, and O. Witzel, *Phys. Rev. D* **91**, 074510 (2015).
- [5] J. A. Bailey *et al.* (Fermilab Lattice and MILC Collaborations), *Phys. Rev. D* **92**, 014024 (2015).
- [6] P. H. Ginsparg and K. G. Wilson, *Phys. Rev. D* **25**, 2649 (1982).
- [7] D. B. Kaplan, *Phys. Lett. B* **288**, 342 (1992).
- [8] Y. Shamir, *Nucl. Phys.* **B406**, 90 (1993).
- [9] V. Furman and Y. Shamir, *Nucl. Phys.* **B439**, 54 (1995).
- [10] R. C. Brower, H. Neff, and K. Orginos, *Comput. Phys. Commun.* **220**, 1 (2017).
- [11] S. Okubo, *Phys. Rev. D* **4**, 725 (1971).
- [12] S. Okubo, *Phys. Rev. D* **3**, 2807 (1971).
- [13] C. G. Boyd, B. Grinstein, and R. F. Lebed, *Nucl. Phys.* **B461**, 493 (1996).
- [14] C. G. Boyd, B. Grinstein, and R. F. Lebed, *Phys. Rev. D* **56**, 6895 (1997).
- [15] I. Caprini, L. Lellouch, and M. Neubert, *Nucl. Phys.* **B530**, 153 (1998).
- [16] C. Bourrely, B. Machet, and E. de Rafael, *Nucl. Phys.* **B189**, 157 (1981).
- [17] C. Bourrely and I. Caprini, *Nucl. Phys.* **B722**, 149 (2005).
- [18] C. Bourrely, I. Caprini, and L. Lellouch, *Phys. Rev. D* **79**, 013008 (2009); **82**, 099902(E) (2010).
- [19] J. A. Bailey *et al.* (Fermilab Lattice and MILC Collaborations), *Phys. Rev. D* **79**, 054507 (2009).
- [20] Y. S. Amhis *et al.* (HFLAV Collaboration), *Eur. Phys. J. C* **81**, 226 (2021).
- [21] Y. Aoki *et al.*, [arXiv:2111.09849](https://arxiv.org/abs/2111.09849); S. Aoki *et al.* (Flavour Lattice Averaging Group), *Eur. Phys. J. C* **80**, 113 (2020).
- [22] P. Gambino, M. Jung, and S. Schacht, *Phys. Lett. B* **795**, 386 (2019).
- [23] M. Wingate, *Eur. Phys. J. A* **57**, 239 (2021).
- [24] S. Gottlieb, *Proc. Sci.*, LATTICE2019 (2020) 275.
- [25] S. Hashimoto, *Prog. Theor. Exp. Phys.* **2017**, 053B03 (2017).
- [26] P. Gambino and S. Hashimoto, *Phys. Rev. Lett.* **125**, 032001 (2020).
- [27] See Supplemental Material at <http://link.aps.org/supplemental/10.1103/PhysRevD.106.054502> for details on the generation of the gauge fields and their properties, and measurements of basic physical quantities.
- [28] G. Burdman, Z. Ligeti, M. Neubert, and Y. Nir, *Phys. Rev. D* **49**, 2331 (1994).
- [29] C. Morningstar and M. J. Peardon, *Phys. Rev. D* **69**, 054501 (2004).
- [30] M. Tomii, G. Cossu, B. Fahy, H. Fukaya, S. Hashimoto, T. Kaneko, and J. Noaki (JLQCD Collaboration), *Phys. Rev. D* **94**, 054504 (2016).
- [31] K. Nakayama, B. Fahy, and S. Hashimoto, *Phys. Rev. D* **94**, 054507 (2016).
- [32] T. Kaneko, B. Colquhoun, H. Fukaya, and S. Hashimoto (JLQCD Collaboration), *EPJ Web Conf.* **175**, 13007 (2018).
- [33] S. Aoki, G. Cossu, H. Fukaya, S. Hashimoto, and T. Kaneko (JLQCD Collaboration), *Prog. Theor. Exp. Phys.* **2018**, 043B07 (2018).
- [34] G. Cossu, H. Fukaya, S. Hashimoto, T. Kaneko, and J.-I. Noaki, *Prog. Theor. Exp. Phys.* **2016**, 093B06 (2016).
- [35] K. Nakayama, H. Fukaya, and S. Hashimoto, *Phys. Rev. D* **98**, 014501 (2018).
- [36] M. Tomii, G. Cossu, B. Fahy, H. Fukaya, S. Hashimoto, T. Kaneko, and J. Noaki (JLQCD Collaboration), *Phys. Rev. D* **96**, 054511 (2017).
- [37] G. P. Lepage, B. Clark, C. T. H. Davies, K. Hornbostel, P. B. Mackenzie, C. Morningstar, and H. Trotter, *Nucl. Phys. B, Proc. Suppl.* **106**, 12 (2002).
- [38] P. Lepage, C. Gohlke, and D. Hackett, [gplepage/gvar](https://github.com/gplepage/gvar): gvar version 11.9.3 (2021).
- [39] P. Lepage and C. Gohlke, [gplepage/lqfit](https://github.com/gplepage/lqfit): lqfit version 12.0 (2021).
- [40] P. Lepage, [gplepage/corrfit](https://github.com/gplepage/corrfit): corrfit version 8.1.1 (2020).
- [41] S. Hashimoto, B. Colquhoun, T. Izubuchi, T. Kaneko, and H. Ohki, *EPJ Web Conf.* **175**, 13006 (2018).
- [42] J. Bijnens and I. Jemos, *Nucl. Phys.* **B840**, 54 (2010); **B844**, 182(E) (2011).
- [43] D. Becirevic, S. Prelovsek, and J. Zupan, *Phys. Rev. D* **67**, 054010 (2003).
- [44] W. Detmold, C. J. D. Lin, and S. Meinel, *Phys. Rev. D* **85**, 114508 (2012).
- [45] H. Ohki, H. Matsufuru, and T. Onogi, *Phys. Rev. D* **77**, 094509 (2008).
- [46] D. Becirevic, B. Blossier, E. Chang, and B. Haas, *Phys. Lett. B* **679**, 231 (2009).
- [47] D. Becirevic and F. Sanfilippo, *Phys. Lett. B* **721**, 94 (2013).
- [48] F. Bernardoni, J. Bulava, M. Donnellan, and R. Sommer (ALPHA Collaboration), *Phys. Lett. B* **740**, 278 (2015).
- [49] J. M. Flynn, P. Fritsch, T. Kawanai, C. Lehner, B. Samways, C. T. Sachrajda, R. S. Van de Water, and O. Witzel (RBC and UKQCD Collaborations), *Phys. Rev. D* **93**, 014510 (2016).
- [50] P. del Amo Sanchez *et al.* (BABAR Collaboration), *Phys. Rev. D* **83**, 032007 (2011).
- [51] C. G. Boyd and M. J. Savage, *Phys. Rev. D* **56**, 303 (1997).
- [52] B. Colquhoun, C. T. H. Davies, R. J. Dowdall, J. Kettle, J. Koponen, G. P. Lepage, and A. T. Lytle (HPQCD Collaboration), *Phys. Rev. D* **91**, 114509 (2015).
- [53] H. Ha *et al.* (Belle Collaboration), *Phys. Rev. D* **83**, 071101 (2011).
- [54] J. P. Lees *et al.* (BABAR Collaboration), *Phys. Rev. D* **86**, 092004 (2012).
- [55] A. Sibidanov *et al.* (Belle Collaboration), *Phys. Rev. D* **88**, 032005 (2013).
- [56] P. A. Zyla *et al.* (Particle Data Group), *Prog. Theor. Exp. Phys.* **2020**, 083C01 (2020).
- [57] A. Biswas, S. Nandi, S. K. Patra, and I. Ray, *J. High Energy Phys.* **07** (2021) 082.
- [58] S. González-Solís, P. Masjuan, and C. Rojas, *Phys. Rev. D* **104**, 114041 (2021).
- [59] D. Leljak, B. Melić, and D. van Dyk, *J. High Energy Phys.* **07** (2021) 036.
- [60] J. Dingfelder and T. Mannel, *Rev. Mod. Phys.* **88**, 035008 (2016).

- [61] W. Detmold, C. Lehner, and S. Meinel, *Phys. Rev. D* **92**, 034503 (2015).
- [62] R. Aaij *et al.* (LHCb Collaboration), *Nat. Phys.* **11**, 743 (2015).
- [63] K. A. Olive *et al.* (Particle Data Group), *Chin. Phys. C* **38**, 090001 (2014).
- [64] G. Cossu, J. Noaki, S. Hashimoto, T. Kaneko, H. Fukaya, P. A. Boyle, and J. Doi, in *Proceedings of the 31st International Symposium on Lattice Field Theory* (2013), arXiv:1311.0084.
- [65] D. Gerosa and M. Vallisneri, *J. Open Source Software* **2**, 222 (2017).